Hydrological Processes

WILEY

RESEARCH ARTICLE OPEN ACCESS

Modelling Glacier Mass Balance and Runoff in the Kaskawulsh River Headwaters of Southwest Yukon, Canada, 1980–2022

Katherine M. Robinson[1] | Gwenn E. Flowers[1] | Michel Baraër[2] | David R. Rounce[3]

[1]Department of Earth Sciences, Simon Fraser University, Burnaby, Canada | [2]Département de génie de la construction, École de Technologie Supérieure, Montréal, Canada | [3]Civil and Environmental Engineering Department, Carnegie Mellon University, Pittsburgh, Pennsylvania, USA

Correspondence: Katherine M. Robinson (kmr18@sfu.ca)

Received: 27 November 2024 | **Revised:** 28 March 2025 | **Accepted:** 24 April 2025

Funding: This work was supported by the Natural Sciences and Engineering Research Council of Canada, Simon Fraser University, Environment and Climate Change Canada, and the National Aeronautics and Space Administration.

Keywords: climate change | glacier runoff | glacierized catchment | peak water | St. Elias Mountains | water budget

ABSTRACT

The highly-glacierized headwaters of the Kaskawulsh River is home to 9% of all glacier ice in Yukon, Canada, and was the source of a sudden meltwater-rerouting event in 2016 that has had significant downstream consequences. We use a distributed mass-balance model driven by downscaled and bias-corrected climate reanalysis data that incorporates observations of sub-debris melt, accumulation, and transient snowline positions to estimate the 1980–2022 glacier mass balance, discharge, and water budget of the Kaskawulsh River headwaters. We estimate a catchment-wide cumulative mass loss of 18.02 Gt over 1980–2022 (-0.38 ± 0.15 m w.e. a^{-1}) and a mean annual discharge of ~60 $m^3\ s^{-1}$, 25% of which originates from non-renewable glacier wastage. The water budget is dominated by glacier ice melt, accounting for 61% of mean annual discharge, followed by snowmelt at 31%, rainfall at 6%, and melt from refrozen ice layers at 2%. Extreme negative and positive mass-balance years produce the largest perturbations in glacier ice melt contributions to the water budget, ranging from a maximum of 67% following negative years to a minimum of 53% in positive years. Trend detection using the Mann-Kendall test shows that catchment-wide annual discharge increased by 3.9 $m^3\ s^{-1}$ per decade from 1980 to 2022, with statistically significant contributions from glacier ice melt (2.8 $m^3\ s^{-1}$ per decade) and rainfall (0.5 $m^3\ s^{-1}$ per decade). Increasing air temperatures and declining spring snowfall have lead to seasonally accelerated snowline retreat, earlier ice exposure, and earlier onset of net ablation in the catchment at a rate of ~5 days per decade. Based on summer air temperatures projected by CMIP6 and the empirical sensitivities of modelled runoff we calculate for 1980–2022, we hypothesise a more than doubling of annual runoff from this catchment by 2080–2100. This result, combined with a decrease in the variability of discharge from glacier ice melt over 1980–2022, suggests that this catchment is unlikely to reach "peak water" (i.e., peak glacier contribution to catchment runoff) this century.

1 | Introduction

Glacier-fed rivers play a critical role in many large-scale drainage basins around the world (e.g., Huss and Hock 2018). In some basins, runoff contributions from glacier-ice melt are expected to increase by the end of the century, whilst other basins are projected to see reductions in runoff from glacier melt associated with declining glacier area (Huss and Hock 2018). Global modelling efforts (e.g., Huss and Hock 2018; Bliss et al. 2014) suggest that this turning point, referred to in the literature as "peak water", has already been reached in nearly half of global glacierized basins, whilst the remaining basins are likely to reach

peak water before the end of the century. Glaciers in Yukon and Alaska are some of the largest contributors to present day global glacier mass loss (Zemp et al. 2019; Hugonnet et al. 2021), and are projected to continue to be amongst the most significant contributors in the future (Rounce et al. 2023). In Yukon, some small watersheds (2%–9% glacierized) have likely already passed peak water (Chesnokova et al. 2020), whilst other large basins like the Alsek River and Yukon River basins, with ~20% glacier cover each, are expected to reach peak water between mid- to late century, depending on the emissions scenario (Huss and Hock 2018).

Here, we employ an existing distributed mass-balance model (Young et al. 2021a; Robinson et al. 2025) to reconstruct four decades of mass balance, runoff, and water budget in a highly-glacierized, ungauged catchment in southwest Yukon. This catchment has, at different times in the recent past, contributed to runoff in both the Yukon River and Alsek River basins (Shugar et al. 2017). Ongoing mass loss throughout this region is producing changes in the timing and magnitude of freshwater that is delivered to the Gulf of Alaska (e.g., Neal et al. 2010), with potentially significant downstream impacts on the sediment and chemical fluxes to near-shore ecosystems (e.g., Hood and Berner 2009) and future salmon habitat quality and range (e.g., Moore et al. 2023; Pitman et al. 2021). With a mean temperature increase of 7.8°C and a 24% increase in annual precipitation projected for northwestern North America by 2081–2100 relative to 1981–2010 under SSP5-8.5 (IPCC 2021), it is important to understand how runoff contributions from highly-glacierized catchments in this region are changing. However, direct observations of glacier runoff via repeated measurements or continuous gauging (e.g., La Frenierre and Mark 2014) are challenging, particularly in remote mountainous catchments, due to the inaccessibility of these sites and the difficulties associated with installing and maintaining gauges in dynamic proglacial streams (e.g., Goss 2021). Modelling approaches that integrate available in situ data offer an alternative method to reconstruct and partition the historical runoff record (e.g., Li et al. 2020; Azam and Srivastava 2020), helping to overcome the limitations of field-based measurements by combining available observations with remote-sensing and climate reanalysis data.

The mass-balance model employed in this study is tailored to the catchment using in situ data and tuned using site-specific remotely-sensed observations (Robinson et al. 2025). It is then used to estimate the catchment-wide annual discharge contributions from ice melt, snowmelt, and rainfall. We analyse trends in the modelled mass balance and discharge and examine correlations between the modelled climate and discharge to identify the drivers of these trends. We also identify factors that produce extremes in the record and use these findings to generate hypotheses about possible future hydrological changes in this regionally significant catchment.

2 | Study Area

The hydrological catchment that encompasses the Kaskawulsh Glacier, hereafter referred to as the Kaskawulsh River headwaters (Figure 1), is a large (1704 km^2), 69% glacierized area located in the St. Elias Mountains of Yukon, Canada, within the Traditional Territories of the Kluane, Champagne & Aishihik, and White River First Nations. The Kaskawulsh Glacier itself is an ~70 km long valley glacier spanning an elevation range of 750–3500 m a.s.l. (Figure S1), and accounts for 93% of the glacierized area in the catchment and ~9% of the glacier-ice volume in Yukon (Farinotti et al. 2019). The Kaskawulsh Glacier is situated on the continental side of the St. Elias Mountains and flows eastward from the ice divide with Hubbard Glacier (Clarke and Holdsworth 2002), with four major tributaries contributing to the main trunk, which terminates at the drainage divide between the Yukon and Alsek River watersheds (Shugar et al. 2017). Approximately 14 other glaciers are located within the catchment, nearly all of which are $< 10\,km^2$ and unnamed.

Ongoing glacier mass loss and retreat in this region have already had pronounced effects on landscape evolution through retreat-driven river reorganisation (e.g., Shugar et al. 2017), and through the formation and growth of new proglacial lakes (e.g., Main et al. 2023). The Kaskawulsh Glacier has been in a state of negative mass balance for several decades, with estimated mass loss rates of 0.46 ± 0.20 m w.e. a^{-1} between 1977 and 2007 (Berthier et al. 2010) and 0.46 ± 0.17 m w.e. a^{-1} between 2007 and 2018 (Young et al. 2021a). An additional 23 km of committed terminus retreat is estimated under the 2007–2018 mean climate (Young et al. 2021a), even without further warming. The glacier has been slow to adjust to its mass imbalance, with just 1.5% reduction in glacier area between 1977 and 2007 and 655 m of terminus retreat from 1956 to 2007 (Foy et al. 2011). Terminus retreat has also been associated with the formation and growth of two proglacial lakes (Shugar et al. 2017; Main et al. 2023). In May 2016, the abrupt drainage of one of these lakes caused meltwater that flowed north via the Ä'äy Chù (Slims River) to Łhù'ààn Mân (Kluane Lake), the Donjek River, White River, Yukon River, and ultimately discharging to the Bering Sea to be diverted south via the Kaskawulsh River (Figure 1), a tributary to the Alsek River that eventually discharges into the Gulf of Alaska (Shugar et al. 2017).

The rerouting event had many downstream consequences, including reduced water levels in Łhù'ààn Mân, and increased dust emissions from the Ä'äy Chù floodplain (e.g., Huck et al. 2023; Bachelder et al. 2020; Shugar et al. 2017). This event was also associated with an increase in braiding intensity and sediment erosion on the Kaskawulsh River, driven by the abrupt increase in discharge (Goss 2021). Prior to the drainage reorganisation, terminus velocities were increasing at an average rate of 3 m a^{-1} per year from 2000 to 2012, but have since rapidly declined at a rate of −12.5 m a^{-1} per year over 2015–2021 (Main et al. 2023). The slowdown and stagnation over parts of the terminus region are believed to be linked to a reduction in flotation caused by the proglacial lake drainage (Main et al. 2023).

3 | Materials and Methods

3.1 | Mass-Balance Model

We use a distributed mass-balance model developed by Young et al. (2021a), with the addition of a surface-elevation parameterization, a glacier-specific representation of sub-debris ablation, and an accumulation bias correction developed for the

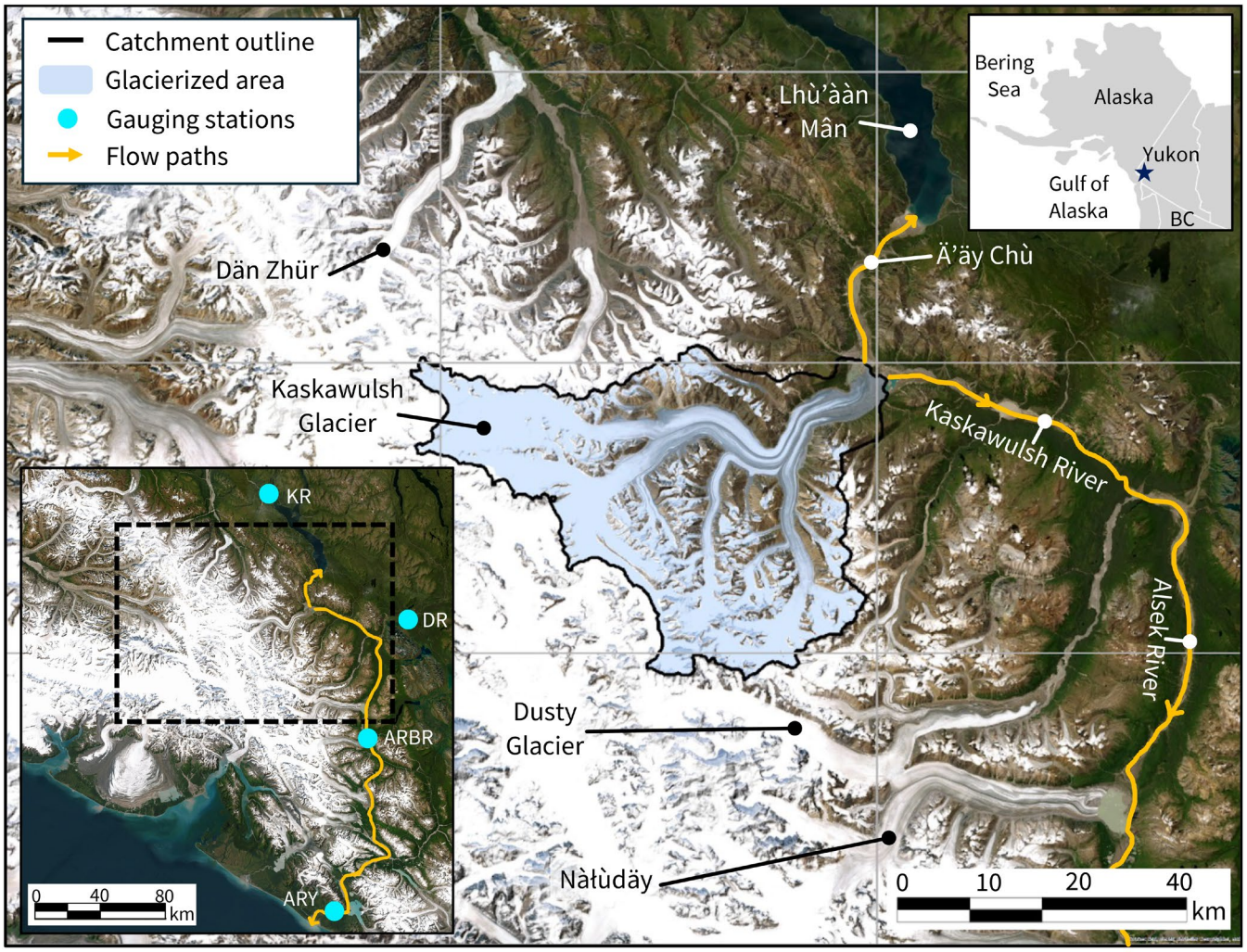

FIGURE 1 | Study area (blue star, inset) and overview of the surrounding glaciers (black text) and hydrological systems (white text). Blue shading indicates the glacierized area, with the boundary of the Kaskawulsh River headwaters outlined in black. Inset at bottom left shows the locations of three hydrometric gauging stations operated by Environment and Climate Change Canada: Kluane River at the outlet of Kluane Lake (KR), Dezadeash River (DR), and Alsek River above Bates River (ARBR), and one station operated by the United States Geological Survey: Alsek River at Dry Bay near Yakutat (ARY). Basemap sources: Esri, Maxar, Earthstar Geographics, and the GIS User Community.

Kaskawulsh River headwaters by Robinson et al. (2025). The climatic mass balance $\dot{b}_{\mathrm{sfc}}(x,y)$ is calculated as the difference between the distributed surface accumulation $\dot{c}_{\mathrm{sfc}}(x,y)$ and distributed surface ablation $\dot{a}_{\mathrm{sfc}}(x,y)$. Ablation is approximated as surface melt minus meltwater that is refrozen. Melt (M; m w.e.) is calculated at a 3-hourly timestep using the enhanced temperature-index model of Hock (1999):

$$M = \begin{cases} \left(\mathrm{MF} + a_{\mathrm{snow/ice}} I\right) T & \text{if } T > 0°C \\ 0 & \text{if } T \leqslant 0°C, \end{cases} \quad (1)$$

where T (°C) is air temperature and I (W m^{-2}) is the potential direct clear-sky solar radiation. The enhanced temperature-index melt model improves upon the classical degree-day model by capturing the influence of topographic shading, slope, and aspect on melt through incorporating the radiation factors ($a_{\mathrm{snow/ice}}$) and potential direct clear-sky solar radiation, the latter of which is calculated using the Hock (1999) shading module. MF (m w.e. 3h^{-1}°C^{-1}), a_{snow} and a_{ice} (m w.e. 3h^{-1}°C^{-1} m^2 W^{-1}) are, respectively, the melt factor and radiation factors for snow and ice which relate melt to temperature and solar radiation, and are empirically determined during a tuning process adopted from Robinson et al. (2025) (see supplementary material for details). The melt-model parameters are tuned to two empirical targets: (a) the 2007–2018 glacier-wide geodetic mass balance (−0.46 ±0.17 m w.e. a^{-1}) estimated by Young et al. (2021a), which primarily serves to constrain the ice radiation factor (a_{ice}), and (b) observed snow cover determined by transient snowline positions delineated from over 50 Landsat-8 and Sentinel-2 satellite images, which primarily serves to constrain the melt factor (MF) and snow radiation factor (a_{snow}) (Robinson et al. 2025). The tuning approach results in 100 different combinations of the melt-model parameters (Table S1), and the mean and standard deviation from this 100-simulation ensemble is presented here.

Meltwater retention is accounted for using a thermodynamic parameterization (see supplementary material for details) to estimate the maximum amount of liquid water (from snowmelt or rainfall) that can be retained in the snowpack via refreezing (Janssens and Huybrechts 2000). Snowmelt and rainfall that do

not refreeze contribute instantaneously to modelled discharge. The impact of supraglacial debris cover on ablation is treated by multiplying the ice melt calculated by Equation 1 by spatially distributed sub-debris melt factors from Robinson et al. (2025), which are largely melt inhibiting over the terminus region of the Kaskawulsh Glacier.

Catchment-wide discharge is the sum of all sources of runoff over the glacierized and non-glacierised areas (e.g., Bliss et al. 2014):

$$Q = M_{\text{glacier ice}} + M_{\text{snow}} + M_{\text{refrozen snowmelt/rain}} + P_l - R, \quad (2)$$

including glacier-ice melt ($M_{\text{glacier ice}}$), snowmelt (M_{snow}), ice melt from the refrozen snowmelt/rain layers formed during previous refreezing events ($M_{\text{refrozen snowmelt/rain}}$), and rainfall ($P_l$), minus the snowmelt and rainfall that are refrozen (R). Ice formed from refrozen snowmelt/rain is treated as superimposed ice in the ablation zone and internal accumulation in the accumulation zone. Snowmelt refers to melt of both the seasonal snowpack and snow accumulation that has persisted from previous seasons, as we do not account for the transition from snow to firn. Snowmelt, rainfall, and refreezing are treated the same over the non-glacierized area as the glacierized area of the catchment. We assume that all runoff instantaneously exits the catchment, that is, we do not account for transit times, supraglacial ponding, or englacial/subglacial storage, all of which would delay or reduce the estimated discharge (e.g., Huss and Hock 2018). Our objective is to examine temporal trends in discharge, rather than to precisely reconstruct the daily discharge timeseries, thus neglecting a time-delay in modelled discharge does not affect the conclusions of the study. Furthermore, without in situ discharge data to constrain the transit time, attempting to reconstruct the daily discharge timeseries would introduce further uncertainty and therefore be only speculative.

We also neglect runoff losses from sublimation, evapotranspiration, and infiltration. Some groundwater may be lost to the Ä'äy Chù, whilst some may resurface proglacially and discharge into the Kaskawulsh River, although these amounts are likely small: in the broader Alsek River Basin, estimated losses due to evapotranspiration and infiltration from non-glacierized areas are 5–40 mm a^{-1}, accounting for 1%–7% of the mean annual precipitation (Chesnokova et al. 2020). Sublimation losses are likely also small. On a small glacier on the northern side of the catchment, a point-scale estimate of sublimation was less than 1% of the total ablation estimated during the 2008 melt season (Wheler and Flowers 2011).

The glacierized area is based on outlines from the Global Land Ice Measurements from Space inventory (GLIMS) Randolph Glacier Inventory (RGI 6.0) (RGI Consortium 2017) (Kaskawulsh Glacier RGI ID: 60-01.16201) and is fixed throughout the simulation period (1980–2022), as the relatively small change in the area of the Kaskawulsh Glacier over recent decades (Foy et al. 2011) suggests that the impact on runoff is minimal. We account for surface lowering over time by updating the elevation of the glacierized area annually based on a smoothed estimate of the average annual elevation-change rate between 1977 and 2018, estimated by Robinson et al. (2025) using Digital Elevation Models (DEMs) from 1977, 2007, and 2018 (see supplementary material).

The model is initialized with an entirely snow-free surface such that all glacierized areas are composed of bare ice. We allow the glacier accumulation area to develop over the first year of the simulation, during which the snowpack builds up and is carried over year to year. This initial spin-up year is discarded from the analysis. The equilibrium line altitude (ELA) and accumulation area ratio (AAR) are transient outputs of the model rather than being prescribed.

3.2 | Climate Data

3.2.1 | Temperature

The temperature and precipitation data used to drive the mass-balance model (Figures 2 and S2) are obtained by downscaling and bias correcting the North American Regional Reanalysis (NARR) dataset (Mesinger et al. 2006). NARR data are available beginning in 1979 and include gridded outputs for a suite of meteorological variables at 3-hourly timesteps on a 32 km × 32 km grid. To obtain the temperature inputs for the melt model, we follow Young et al. (2021a) in downscaling NARR temperature data to a 200 m grid using a linear regression scheme from Jarosch et al. (2012) to correlate NARR air temperatures and geopotential heights within the lower layer of the atmosphere and estimate the local lapse rate and sea-level air temperature at each 32 × 32 km NARR gridcell. The lapse rates and sea-level air temperatures from the linear regression are bilinearly interpolated across the model domain and used to calculate the 2-m air temperature at the elevation of each gridcell. Downscaled NARR temperature data for the St. Elias Mountains have been extensively validated by Williamson et al. (2020), who used the same downscaling approach for the period 1979–2016, showing very high correlations with air temperature measurements from 15 meteorological stations spanning 599–5340 m a.s.l. Downscaled NARR temperatures are then bias-corrected using monthly correction factors derived from eight automatic weather station records from in and around the Kaskawulsh River headwaters by Young et al. (2021a).

3.2.2 | Precipitation

The precipitation downscaling procedure follows a regression-based approach from Guan et al. (2009), adopted by Young et al. (2021a), that relates NARR surface precipitation to the geographic predictors of precipitation (Easting, Northing and elevation) from 13 NARR gridcells on the continental side of the St. Elias Mountains and orographic divide (Robinson 2024). Accumulation is estimated from 200 m downscaled NARR precipitation partitioned into rain and snow using a prescribed temperature threshold of 1°C (Young et al. 2021a). Downscaled accumulation is bias corrected with an elevation-dependent function developed by Robinson et al. (2025) using 27 in situ measurements of snow depth and density made between 2007 and 2022 at 18 different locations

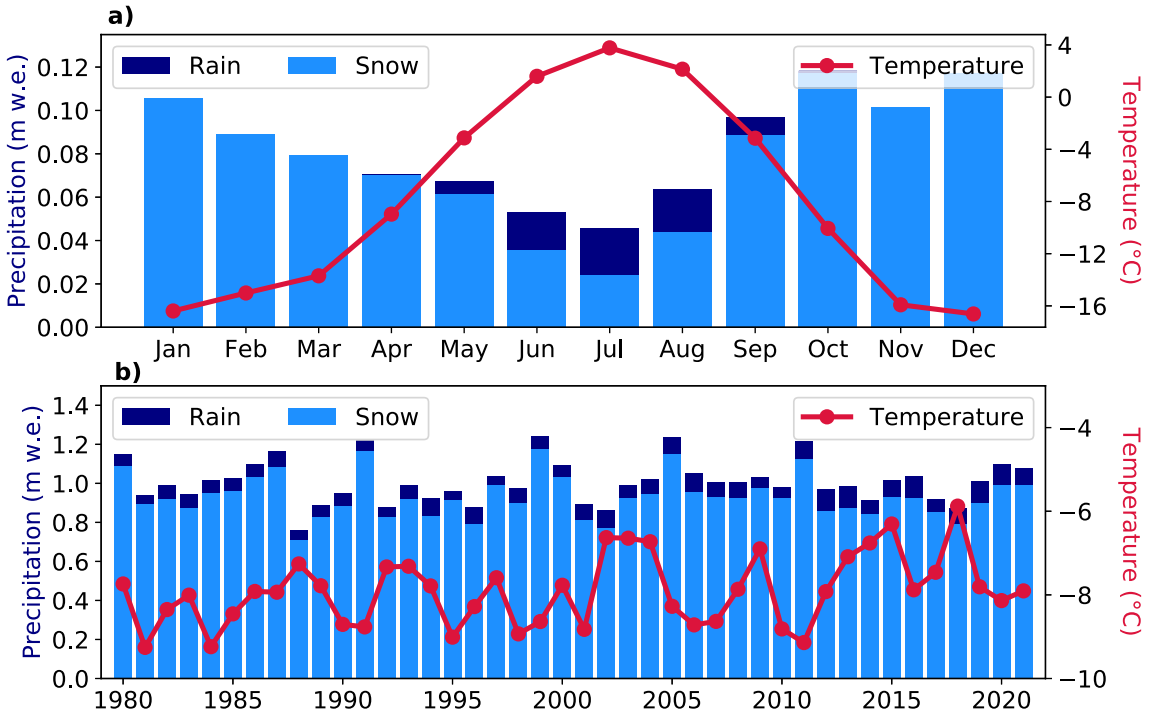

FIGURE 2 | Downscaled and bias corrected North American Regional reanalysis data averaged over the Kaskawulsh River headwaters. (a) Monthly average temperature (red line) and precipitation partitioned into snow and rainfall using a temperature threshold of 1°C (light blue: snow, dark blue: rainfall). (b) Mean annual temperature and total precipitation from 1980 to 2022. Note that units for precipitation are metres water equivalent (m w.e.), representing the volume of water divided by the catchment area. The distributed climate inputs and mean annual precipitation as a function of elevation are shown in Figures S2 and S3.

within the catchment between 1220 and 2670 m a.s.l. These in situ measurements are primarily located along the main trunk and Central Arm of the Kaskawulsh Glacier, with two measurements located on the South Arm of the glacier and several others located on smaller glaciers on the north side of the catchment. Downscaled NARR data generally underestimate the measured seasonal accumulation in the catchment, with the ratio of measured to downscaled accumulation generally increasing with elevation. NARR data were also found to underestimate precipitation in mountainous regions in British Columbia, which may be due to sparse meteorological observations at high elevations in mountain regions and the exclusion of Canadian precipitation gauge data from the NARR data assimilation process beginning in 2003 (Hunter et al. 2020). Robinson et al. (2025) showed that applying the elevation-dependent correction factors to downscaled NARR accumulation leads to improved agreement with airborne-radar-derived accumulation estimates from NASA's Operation IceBridge (OIB) survey of the Kaskawulsh Glacier in May 2021 (Li et al. 2023), with a 67% reduction in the mean absolute error between measured and modelled accumulation relative to downscaled, uncorrected accumulation data. In the absence of reliable in situ rainfall data, the liquid component of downscaled precipitation is not bias corrected.

3.3 | Hydrological Data

Discharge from the Kaskawulsh River headwaters catchment historically flowed into two drainage basins: the Yukon River basin to the north via Ä'äy Chù and the Alsek River basin to the south via Kaskawulsh River (Figure 1). In May 2016, the retreat of Kaskawulsh Glacier triggered a drainage reorganisation in which melt water from the Ä'äy Chù was captured by the Kaskawulsh River, which has a lower base level than the Ä'äy Chù, ultimately increasing the supply of water to the Alsek River (Shugar et al. 2017). We estimate the contribution of the Kaskawulsh River headwaters catchment to discharge on the Alsek River since the 2016 drainage reorganisation using discharge data from two downstream hydrometric stations. Neither the Kaskawulsh River nor the Ä'äy Chù is gauged near the glacier terminus, precluding direct comparisons between modelled and measured discharge from the catchment.

Environment and Climate Change Canada (ECCC) maintains a hydrometric station on the Alsek River above Bates River (60.118°N, −137.978°W), located just above Fisher Glacier, roughly 110 km downstream from the Kaskawulsh Glacier terminus (Figure 1). The gross drainage area at this location is 16 200 km^2, and includes other large glaciers south of the Kaskawulsh Glacier, such as Dusty Glacier and Nàłùdäy (Lowell Glacier). Daily discharge measurements at this station are available from 1974 to 2019. The ECCC Historical Hydrometric Data website notes that particularly high flows were recorded in 2016 after meltwater from the Kaskawulsh Glacier was rerouted to the Alsek River. The drainage area also includes the Dezadeash River catchment (8450 km^2), a tributary catchment to the Alsek River where discharge is artificially controlled for hydroelectricity production.

Another hydrometric station operated by the United States Geological Survey (USGS) is located about 160 km further

downstream from the Bates River junction with the Alsek River at 59.192°N, −138.333°W (Figure 1). This station is located at Dry Bay near Yakutat, Alaska, about 22 km upstream of where the Alsek River discharges to the North Pacific Ocean, and has a gross drainage area of 29 570 km^2.

3.4 | Trend Detection

Hydrological changes over the four-decade study period are identified by examining the absolute and relative contributions to total discharge from each modelled source: glacier-ice melt, snowmelt, rainfall, and melt of ice formed from refrozen snowmelt/rain over time. We apply the Mann-Kendall and Modified Mann-Kendall statistical tests to the modelled discharge timeseries over 1980–2022 to identify the significance and magnitude of these changes.

The Mann-Kendall test is a non-parametric test used to identify monotonic positive or negative trends in a timeseries (Kendall 1948; Mann 1945). The test, based on the relative differences between pairs of observations (ranks), reduces the influence of outliers in the data but relies on the assumption that the observations are independent of one another. Positive serial correlation between successive values can therefore bias this test, and is accounted for in the Modified Mann-Kendall test by adjusting the sample size of the data to reflect the fact that not all values in the timeseries are independent of one another (Hamed and Rao 1998). As a result, the Modified Mann-Kendall test has a decreased rate of falsely identifying trends in autocorrelated data compared to the original Mann-Kendall test. We reject the null hypothesis, which assumes no monotonic trend in the timeseries, based on the arbitrary but common significance level of $\alpha = 0.05$. The magnitude of statistically significant trends is estimated using Sen's slope, which is commonly used in conjuction with the Mann-Kendall test, and is the median slope between all possible pairs of data points in the timeseries, resulting in an estimate that reduces the influence of outliers (Sen 1968).

Following Chesnokova et al. (2020), we apply the Mann-Kendall and Modified Mann-Kendall statistical tests to a suite of variables that characterise the hydrological regime of the catchment (Table 1), and consider the results of both tests to identify persistent trends in discharge over time. We evaluate the mean discharge over key seasonal periods and the timing of the onset of the ablation season and peak discharge to detect shifts in the seasonal discharge pattern. We also assess trends in discharge variability across different time frames to evaluate whether the catchment has passed the peak water threshold. Decreased variability in conjunction with increased ablation-season discharge may suggest that a catchment is headed towards peak water, with increasing influence from the glacierized area, whilst increased variability with decreased discharge may indicate that peak water has passed, leading to less predictable runoff as glacier ice melt declines (e.g., Baraër et al. 2012; Chesnokova et al. 2020).

3.5 | Estimating Future Changes in Discharge

We examine the relationships between modelled discharge and changes in the mass balance and climate over the study period to identify possible drivers of changes to the hydrological regime. To assess the strength of any relationship between two variables, we apply Spearman's correlation test, another non-parametric test based on the correlation between ranks of pairs of observations (Spearman 1904). Relationships that exhibit statistically significant correlations are used to compute the sensitivity of modelled discharge to changes in the mass balance and/or climate over the study period. We estimate trend magnitudes between significantly correlated variables using a linear regression and use these historical sensitivities to generate hypotheses about possible futures for the hydrological regime and water budget of the catchment.

TABLE 1 | Variables used to identify hydrological changes over time, computed from the modelled daily discharge timeseries.

Variable	Description	Units
Q_{annual}	Mean discharge over the hydrological year (Oct–Sept)	$m^3 s^{-1}$
Q_{abl1}	Mean July–August discharge	$m^3 s^{-1}$
Q_{abl2}	Mean May–August discharge	$m^3 s^{-1}$
Q_w	Mean winter discharge (November–March)	$m^3 s^{-1}$
Q_{max5d}	Mean 5-day maximum discharge	$m^3 s^{-1}$
D_{max5d}	Day of year corresponding to Q_{max5d}	Day of year
D_{abl}	The first day of the year with a daily discharge $> 0 m^3 s^{-1}$	Day of year
CV_{annual}	Coefficient of variation for Q_{annual}	Unitless
CV_{abl1}	Coefficient of variation for Q_{abl1}	Unitless
CV_{abl2}	Coefficient of variation for Q_{abl2}	Unitless

To estimate future changes in climate in the study area, we use the results of the Coupled Model Intercomparison Project Phase 6 (CMIP6) for SSP5-8.5, a high-emissions scenario that represents the highest warming by 2100 of all CMIP6 scenarios (Gidden et al. 2019), and allows us to explore the maximum impact of climate change on discharge in the catchment within the bounds of CMIP6. Whilst individual CMIP6 model projections are subject to significant uncertainties, particularly at the glacier scale due to the coarse resolution of general circulation models, using an ensemble of models helps to mitigate these uncertainties by capturing a range of potential future changes forced by state-of-the-art climate-model projections. We extract projected changes for the Kaskawulsh River headwaters from the 1°×1° CMIP6 gridcell with the greatest overlap with the catchment for three future time periods: near-term (2021–2040), medium-term (2041–2060), and long-term (2081–2100) relative to the historical period 1981–2010 (Gutiérrez et al. 2021). We then multiply the historical sensitivity to various climate variables by the projected change in any given variable for the three future time periods. The resulting change in discharge is added to the average discharge from 1981 to 2010 (estimated with the mass-balance model) to generate estimates about future hydrological changes in the catchment.

4 | Results

4.1 | Kaskawulsh River Headwaters Mass Balance, Discharge, and Water Budget From 1980 to 2022

Using the tuned mass-balance model, we reconstruct the 1980–2022 mass balance and discharge record from the Kaskawulsh River headwaters. We estimate that the cumulative mass loss from all ice in this catchment between 1980 and 2022 amounted to 18.02 Gt (Figure 3a), with an average mass balance of −0.40 ± 0.16 m w.e. a^{-1} from the Kaskawulsh Glacier alone and −0.38 ± 0.15 m w.e. a^{-1} from all ice in the catchment. For several of the smaller glaciers on the periphery of the catchment, the model incorrectly predicts positive mass balances over the study period (e.g., Larsen et al. 2015), an artefact caused by the fact that none of the tuning data pertain to these small glaciers. However, these glaciers represent just 6.3% of ice in the catchment by area and cannot compensate for the negative balance estimated for the Kaskawulsh Glacier.

In each decade since the 1980s, the mean annual mass balance of the Kaskawulsh Glacier has become more negative (Table 2), indicating that mass loss may be accelerating. The seasonal onset of net ablation in the catchment, defined by the date where the annual (1 Oct–30 Sept) cumulative balance becomes negative, occurs by 28 July on average, however our modelling results suggest that the timing of this transition is occurring earlier in the melt season by approximately five days per decade (Figure S4), and occurred as early as 28 June during the most negative balance year (–1.41 m w.e. a^{-1} in 2003–2004; Figure 3b).

Several years during the study period had net positive mass balances (Figure 3b), especially during the period 1980–1988 when the net balance of the catchment was frequently near equilibrium

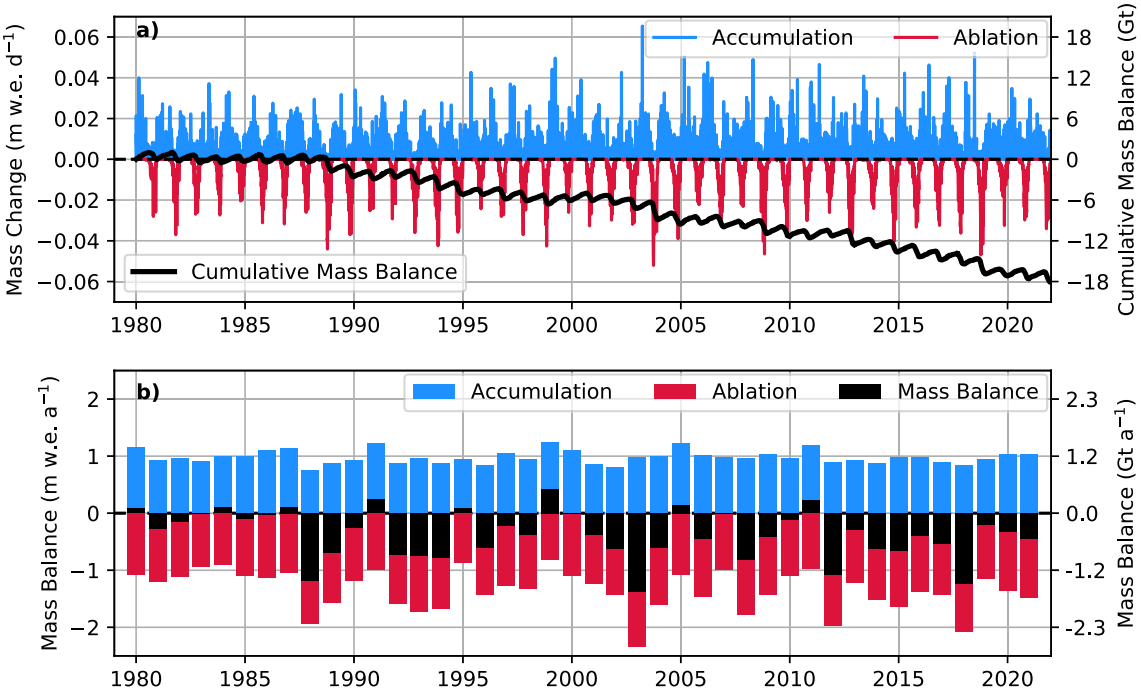

FIGURE 3 | Timeseries of daily and annual mass-balance components from 1980 to 2022. (a) Daily mean accumulation (blue) and ablation (red) over the glacierized area in the Kaskawulsh River headwaters catchment, and the cumulative mass balance (black) from 1980 to 2022 (– 18.02 Gt). (b) Annual glacierized area-wide mean accumulation, ablation, and mass balance.

TABLE 2 | Mean mass balances from the Kaskawulsh Glacier alone and catchment-wide glacierized area (including Kaskawulsh Glacier).

	Kaskawulsh Glacier mass balance (m w.e. a^{-1})	Catchment-wide mass balance (m w.e. a^{-1})	Total mass change (Gt)
1980–1989	−0.25 ± 0.14	−0.22 ± 0.13	−2.54 ± 1.55
1990–1999	−0.32 ± 0.15	−0.30 ± 0.14	−3.48 ± 1.69
2000–2009	−0.48 ± 0.17	−0.45 ± 0.16	−5.30 ± 1.93
2010–2019	−0.53 ± 0.18	−0.49 ± 0.17	−5.80 ± 1.97
2020–2022	−0.42 ± 0.16	−0.39 ± 0.16	−0.91 ± 0.37
1980–2022	**−0.40 ± 0.16**	**−0.38 ± 0.15**	**−18.02 ± 7.51**

Note: Uncertainties reported are the standard deviations of the 100 simulations that comprise the tuned mass-balance model.

with an average mass balance of −0.04 m w.e. a^{-1}. This trend is potentially linked to the Pacific Decadal Oscillation (PDO) (e.g., Brabets and Walvoord 2009); there was a strong positive modal shift in the PDO index in 1976 which became briefly negative again around August 1988 (Mantua and Hare 2002). Similar positive trends in accumulation and mass balance were observed in Yukon and Alaska during the same set of years (Foy et al. 2011). For instance, Wolverine Glacier in southern Alaska experienced a mass gain of 5.9 m w.e. between 1976 and 1988 before transitioning to a period of nearly continuous mass loss (Josberger et al. 2007). However, the relationship between winter accumulation and the PDO remains ambiguous. In contrast to the positive mass-balance trend in the Kaskawulsh River headwaters following the positive PDO shift, Criscitiello et al. (2010) showed that the mass balances of Taku and Lemon Creek Glaciers in the Juneau Icefield are negatively correlated with the PDO, with the positive phase generally associated with negative mass balances in this region. The Kaskawulsh River headwaters last experienced a positive net mass balance during the 2011–2012 balance year, making the past decade (2012–2022) the longest period of consecutive negative balance years in the study period by a factor of two (Figure 3b).

Modelled discharge (Equation 2) is partitioned into four sources: glacier-ice melt, net snowmelt (total snowmelt minus refreezing), net rainfall (total rainfall minus refreezing), and melt from the refrozen snowmelt/rain layer. Early in the ablation season (late-April until approximately mid-June), the water budget is primarily influenced by snowmelt (Figure 4b). Over the course of the ablation season however, glacier-ice melt becomes the predominant source of discharge, accounting for an average of 61% of the annual discharge, whilst snowmelt accounts for 31%, rainfall 6%, and melt of refrozen snowmelt/rain 2% (Figure 4b). Each source of discharge has a strong elevation-dependence, with no runoff originating at elevations greater than ~3000 m a.s.l. due to the refreezing of meltwater and rainfall (Figure S5). Mean annual discharge from non-renewable glacier wastage (melt in excess of annual accumulation) is 14.9 m^3 s^{-1}, accounting for ~25% of the total mean annual discharge (59.9 m^3 s^{-1}) on average between 1980 and 2022. However, in the three most negative mass-balance years, discharge from non-renewable glacier wastage makes up > 50% of the annual discharge.

4.2 | Contributions to the Alsek River

Mean annual discharge recorded at the hydrometric station on the Alsek River above Bates River (Figure 1) during the decade preceding the rerouting of melt water from Kaskawulsh Glacier (2005–2015) was 248.6 m^3 s^{-1}. This increased to 321.5 m^3 s^{-1} (+72.9 m^3 s^{-1}) in 2016–2019 after melt water that previously entered the Ä'äy Chù was diverted south to the Kaskawulsh River, which flows into the Alsek River (Figure S6). We estimate the mean annual discharge from the Kaskawulsh River headwaters from 2016 to 2019 to be 72.0 ± 25.4 m^3 s^{-1}, consistent with the observed increase in discharge in the Alsek River after the drainage reorganisation. This supports the idea that the observed increase in discharge on the Alsek River was driven by the hydrological reorganisation, rather than natural variability in the downstream climatic conditions. Modelled discharge in the Kaskawulsh River headwaters over the 2015–2016 hydrological year was 71.7 m^3 s^{-1}, considerably higher than the historic (1980–2015) modelled annual discharge of 58.3 m^3 s^{-1} (Figure 4a). Indeed Shugar et al. (2017) hypothesised that warmer than average air temperatures and enhanced surface melt during the 2016 melt season led to the development

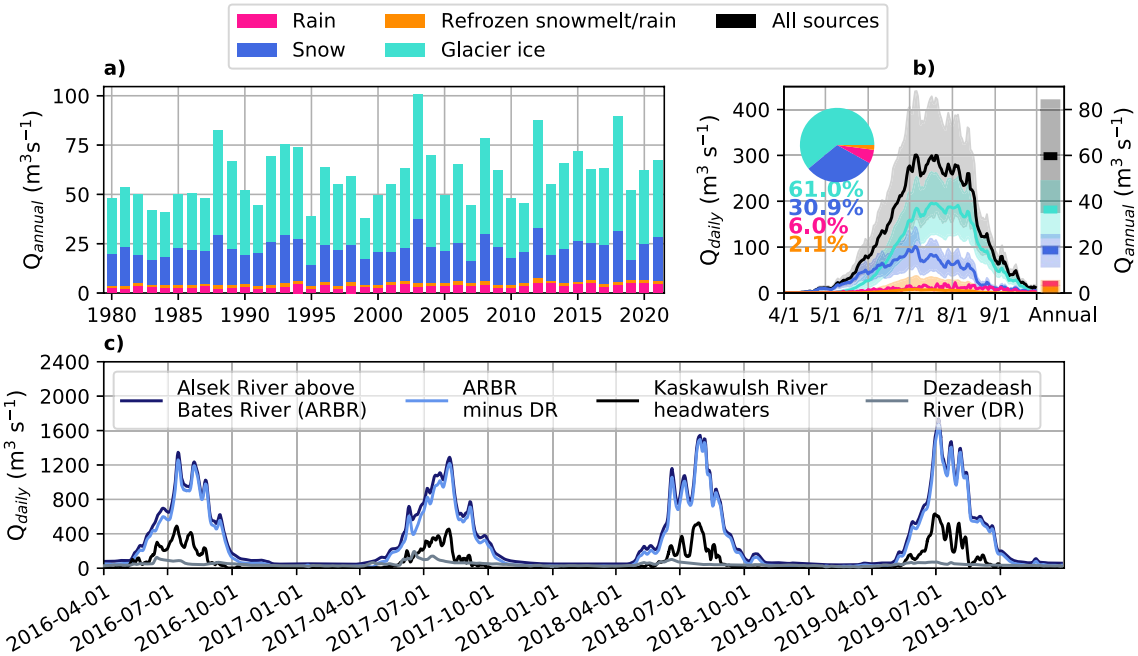

FIGURE 4 | Catchment-wide annual discharge and mean daily discharge from the four modelled sources from 1980 to 2022 (Equation 2). (a) Annual discharge and (b) mean daily discharge from 1980 to 2022. Pie chart and percentages represent the fractional contributions from each source to total catchment-wide discharge, whilst bars on the right *y*-axis show the mean annual discharge from each source. Shading shows the standard deviation of the 100-simulation ensemble that comprise the tuned mass-balance model. (c) Daily modelled discharge from the Kaskawulsh River headwaters (this study, black line) and discharge measured at two downstream hydrometric stations.

and enlargement of an ice-walled channel connecting the two proglacial lakes, causing one of the proglacial lakes that previously drained into the Ä'äy Chù to drain into to the lower base-level Kaskawulsh River (Figure 1).

The Kaskawulsh River headwaters (1704 km^2) represent just over 10% of the total drainage area of the Alsek River above Bates River station (16 200 km^2), or 22% of the drainage area of the Alsek River above Bates River station if the Dezadeash River drainage (8450 km^2), a tributary to the Alsek River where discharge is artificially controlled for hydroelectricity production, is excluded. Modelled annual discharge from the Kaskawulsh River headwaters accounts for 19%–26% of the annual discharge measured at the Alsek River above Bates River hydrometric station between 2016 and 2019. Modelled contributions are largest in July when glacier-ice melt typically reaches a peak, amounting to 32% of the July discharge measured at the gauging station (Figure S7). Subtracting the annual discharge contributions from the Dezadeash River station (Figure 1), the estimated annual discharge from the Kaskawulsh River headwaters account for 22%–29% of the annual discharge measured at the Alsek River above Bates River station (Figure 4c). The Kaskawulsh River headwaters also have a high specific discharge (0.042 $m^3\ s^{-1}\ m^{-3}$) relative to the drainage area of the Alsek River above Bates River station (0.020 $m^3\ s^{-1}\ m^{-2}$), likely due to the high fraction of glacierized area in the catchment. Whilst modelled discharge cannot be verified without direct measurements at the Kaskawulsh River headwaters, considering the substantial size of Kaskawulsh Glacier (1099 km^2) relative to the other major glaciers upstream of the ECCC hydrometric station, namely Dusty Glacier (343 km^2) and Nàłùdäy (Lowell Glacier) (582 km^2) (Arendt et al. 2017) and that the modelled relative contribution from the Kaskawulsh River headwaters is proportional to the fraction of the drainage area it represents, these estimations of discharge appear reasonable. We provide a qualitative indicator of model performance for the 2018–2019 hydrological year, which had particularly high summer melt, by comparing modelled daily discharge to daily discharge measured at the downstream hydrometric stations (Figure S8). Using cross-correlation to estimate the time delay between modelled discharge for the Kaskawulsh River headwaters and discharge measured at downstream stations, we find the maximum correlation ($r = 0.92$) with a two-day lag at the Alsek River above Bates River station (110 km downstream from the Kaskawulsh Glacier terminus), and a three-day lag ($r = 0.85$) at the Alsek River at Dry Bay near Yakutat station (270 km downstream from the Kaskawulsh Glacier terminus) (Figure 1).

Relative to the period 1980–1989, catchment-wide annual discharge increased by 6.5%, 18.9%, and 19.5% in each subsequent decade during the study period (Table S2). This increasing trend in modelled discharge is consistent with the trend in observed discharge downstream at the Alsek River above Bates River station, suggesting that the climatic changes driving increased discharge in the catchment affected discharge downstream as well (Figure S9). Relative to the mean annual discharge from 1980 to 1989 at the Alsek River above Bates River station (219.1 $m^3\ s^{-1}$), annual discharge at the station increased by 2.8% (225.1 $m^3\ s^{-1}$), 13.0% (247.6 $m^3\ s^{-1}$), and 27.5% (279.4 $m^3\ s^{-1}$) in each subsequent decade. If we subtract the modelled contributions from the Kaskawulsh River headwaters after 2016, discharge at the Alsek River above Bates River station still increased by 14.5% (cf. 27.5%) during 2010–2019 relative to 1980–1989.

Further downstream at the USGS hydrometric station on the Alsek River at Dry Bay near Yakutat (Figure 1), annual discharge recorded after the hydrological rerouting (2016–2022) was 1328.1 $m^3\ s^{-1}$. Based on these values, we estimate that the annual discharge from the Kaskawulsh River headwaters (66.9 $\pm$ 26.6 $m^3\ s^{-1}$ as modelled over 2016–2022) accounts for 3%–7% of to the total annual discharge to the North Pacific Ocean from the Alsek River.

4.3 | Changes in Hydrological Regime

4.3.1 | Shifts in Glacier Ice Melt Indicate Pre-Peak Water Phase

Catchment-wide annual discharge (Q_{annual}) increased at a statistically significant rate of 3.9 $m^3\ s^{-1}$ per decade from 1980 to 2022 ($p = 0.006$), whilst mean May–August discharge (Q_{abl2}) also increased significantly by 10.2 $m^3\ s^{-1}$ per decade ($p = 0.007$) (Figure 5). A large fraction of this increase in annual discharge is due to enhanced glacier-ice melt: both the Mann-Kendall and Modified Mann-Kendall tests found positive trends in mean annual discharge (Q_{annual}), mean July–August discharge (Q_{abl1}), and mean May–August discharge (Q_{abl2}) from glacier-ice melt, the latter of which exhibits a statistically significant increase of 7.7 $m^3\ s^{-1}$ per decade ($p = 0.003$) based on the Modified Mann-Kendall test (Figure 5). In addition, the mean 5-day maximum discharge ($Q_{max\ 5d}$), a measure of peak annual discharge, from glacier-ice melt exhibits a statistically significant increase of 9.8 $m^3\ s^{-1}$ per decade ($p = 0.000001$). Interannual discharge variability from glacier-ice melt (CV_{annual}) decreased at a statistically significant rate ($p = 0.00006$) (Figure 5), characteristic of a catchment in the early stages of deglaciation (Baraër et al. 2012). These patterns suggest that glacier-ice melt is exerting an increasing influence on catchment-wide discharge over time, as evidenced by both the increase in discharge and decrease in interannual discharge variability.

Increased ice melt may be explained in part by the increase in summer air temperatures over 1980–2022 (+0.019°C a^{-1}, $p = 0.12$). Decreased April snowfall (−0.65 mm w.e.,$month^{-1}$, $p = 0.03$) (Figure 6b) may also lead to accelerated snowline retreat and earlier ice exposure in the melt season (Figure 6d), whilst increased snowfall in August and September (Figure 6b) can inhibit melt due to the additional snow cover reducing the exposure of glacier ice to radiation.

The model results suggest that early spring glacier-ice melt is increasing at a greater pace than late summer glacier-ice melt, producing an asymmetric shift in the seasonal discharge regime from glacier-ice melt (Figure 6e). Whilst we find no significant trend in the timing of peak discharge ($D_{max\ 5d}$), the date when discharge from glacier-ice melt begins (D_{abl}) exhibits a statistically significant shift ($p = 0.00002$), occurring earlier in the melt season by about 3.5 days per decade (Figure 5), consistent with the aforementioned increase in early summer ice melt (Figure 6e).

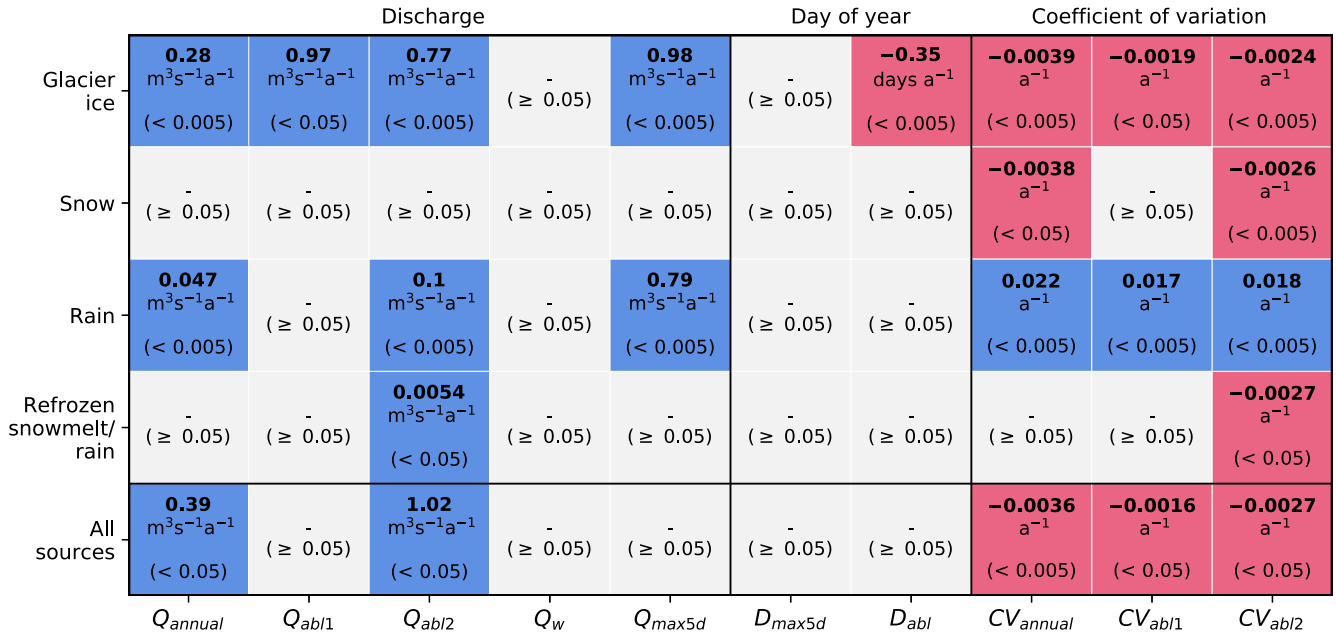

FIGURE 5 | Results of the modified Mann-Kendall test applied to the computed discharge variables (Table 1): Q_{annual} (mean annual discharge), Q_{abl1} (mean July–August discharge), Q_{abl2} (mean May–August discharge), Q_w (mean November–March discharge), $Q_{max\ 5d}$ (mean 5-day maximum discharge), $D_{max\ 5d}$ (day of year corresponding to $Q_{max\ 5d}$), D_{abl} (first day of year with daily discharge > 0), CV_{annual} (coefficient of variation for Q_{annual}), CV_{abl1} (coefficient of variation for Q_{abl1}), and CV_{abl2} (coefficient of variation for Q_{abl2}). Blue squares indicate a statistically-significant positive trend, whilst red squares indicate a statistically-significant negative trend. Grey squares indicate no statistically-significant trend. Values reported inside each square are the magnitude of the trend (for statistically-significant trends only), with *p*-values in parentheses. See Figure S10 for the original Mann-Kendall test results.

4.3.2 | Trends in Discharge From Snowmelt and Rainfall

Monthly discharge from snowmelt (Figure 6f) fluctuates following the observed trends in temperature (Figure 6a), rather than exhibiting monotonic trends like those observed in glacier-ice melt (Figure 6e,f). This suggests that discharge from snowmelt is closely related to the available melt energy. In accordance with the observed trend in positive degree-days in May (Figure 6a), snowmelt in May increased monotonically over each decade of the study period. However, there are no statistically significant trends in mean discharge from snowmelt over July–August (Q_{abl1}) or May–August (Q_{abl2}) (Table 1, Figure 5).

Although snowmelt accounts for 20%–39% of the annual water budget between 1980 and 2022 (Figure 4a), its relative importance may decrease over time due to the increased contributions from glacier-ice melt. Though the catchment-wide average annual snowfall may have decreased slightly over the study period (−0.001 m w.e. a^{-1}), the trend is not statistically significant ($p = 0.38$). The catchment-wide average fraction of annual precipitation occurring as rain, however, has increased at a statistically significant rate of ~1% per decade (+0.001 m w.e. a^{-1}, $p = 0.00007$) between 1980 and 2022 (Figure S12). Annual discharge from rainfall, which makes up 2%–11% of the annual catchment-wide water budget, increased 57% from 2.8 $m^3\ s^{-1}$ in 1980–1989 to 4.4 $m^3\ s^{-1}$ in 2010–2019, with particularly substantial increases in August and September (Figure 6g) in part due to increased air temperatures impacting the partitioning of precipitation into rain and snow during late summer/early fall. These changes point to rainfall becoming a more important contributor to discharge in the future. In contrast to glacier ice melt, rainfall saw an increase in discharge variability between 1980 and 2022, a trend consistent with an increase in rainfall intensity over the study period.

4.4 | Drivers of Extremes in the Water Budget and Discharge Record

4.4.1 | Impact of Mass Balance on the Water Budget

Extreme negative mass-balance years (defined as annual mass balances in the bottom 5% of the study period) range from −1.23 to −1.41 m w.e. a^{-1}, whilst extreme positive mass-balance years (defined as the top 5%) range from 0.20 to 0.41 m w.e. a^{-1}. Extreme negative years influence the catchment-wide water budget in the subsequent year through preconditioning the glacier surface for enhanced firn (treated as snow in the model) or ice melt. During a year with an extreme negative mass balance there is reduction in the accumulation area, resulting in an increase in the relative contribution of glacier-ice melt to the water budget during the subsequent year (e.g., Figure 7). This preconditioning effect occurs even when the subsequent year's mass balance returns to a value closer to the long-term average. Though we do not explicitly account for firn in this model, this effect captures the change in the water budget that would occur as firn/ice above the ELA is exposed.

For example, following the 2003–2004 mass-balance year, which was the most negative in the record and had a greatly reduced AAR (48.6%) compared to the mean 1980–2022 AAR (62.9%) (e.g., Figure 7c), the fractional contribution from ice melt increased by

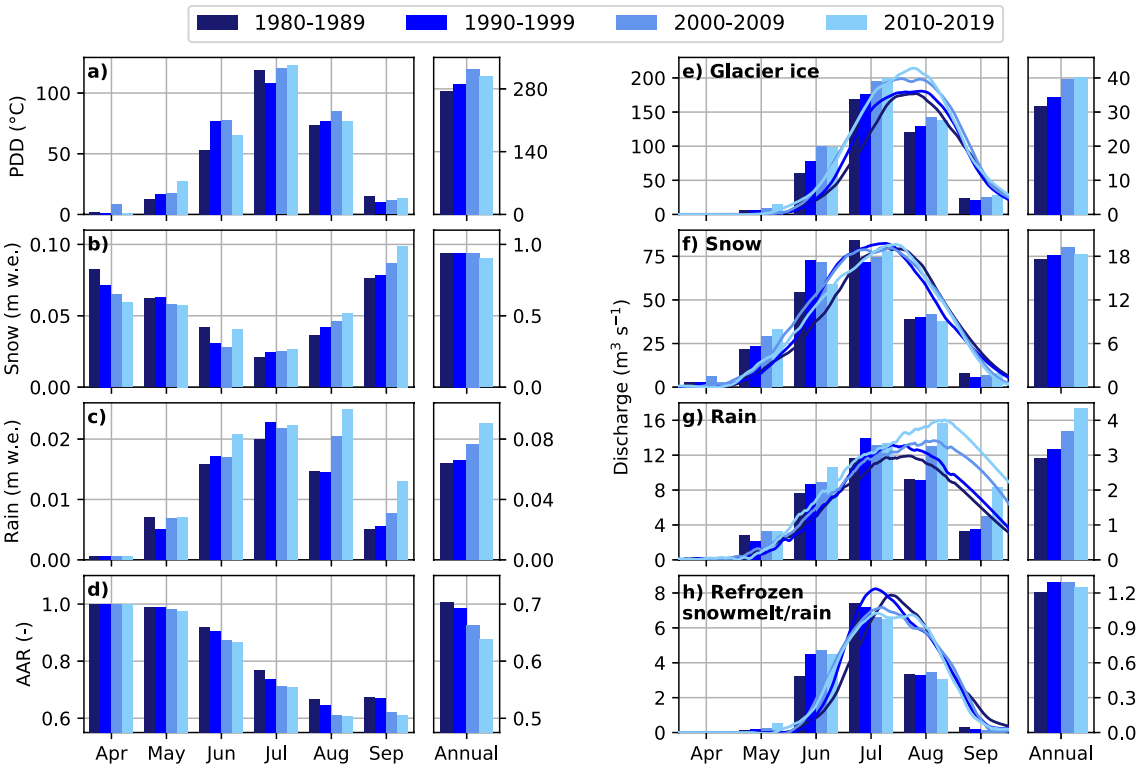

FIGURE 6 | Trends in climate, mass-balance, and discharge variables during the study period. (a–d) Monthly and annual (a) positive degree-day sum (PDD), (b) snowfall, (c) rainfall computed from downscaled and bias-corrected NARR precipitation partitioned into rain and snow using a temperature threshold of 1°C, and (d) transient accumulation area ratio (AAR). See Figures S11 and S12 for timeseries of these trends over 1980–2022. July 1988 was anomalously warm, without which the 1980–1989 average PDD in (a) would be lower than the 1990–1999 average. Units for precipitation in (b, c) are metres water equivalent (m w.e.), representing the volume of water divided by the catchment area (i.e., the thickness of water distributed over the catchment area). (e–h) Catchment-wide monthly and annual discharge (bars), with decadally averaged daily discharge (lines) smoothed using a zero-phase-shift filter and a window size of 51 days (91 days for rainfall) (Figure S13). Note the difference in scales on the *y*-axes in (e–h).

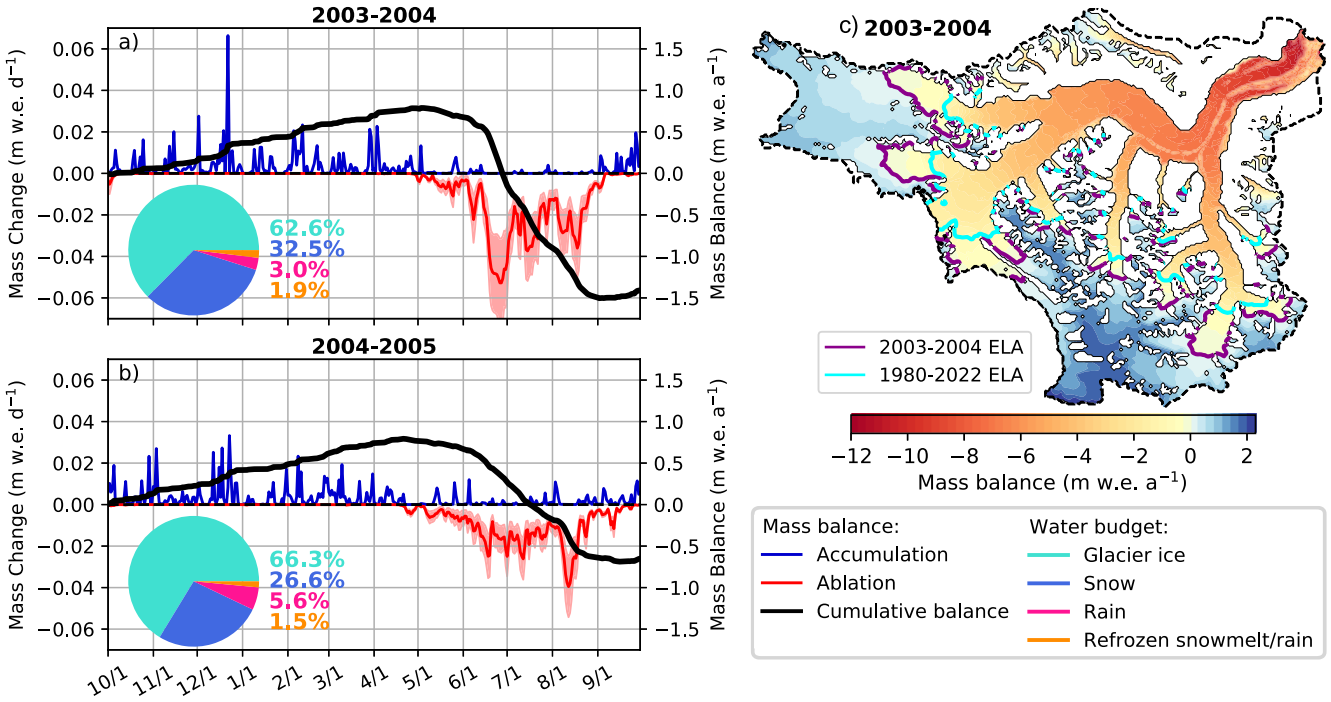

FIGURE 7 | Cumulative mass balance (black curves) and water budgets (pie charts) corresponding to (a) the most negative mass-balance year between 1980 and 2022 (2003–2004: −1.41 m w.e. a^{-1}), and (b) the following year. (c) The distributed mass balance for the 2003–2004 hydrological year (1 Oct–30 Sept), with the 2003–2004 modelled ELA (purple line) compared to the long-term modelled ELA (cyan line). See Figures S14–S19 for additional examples of water budgets following the most positive and negative mass-balance years.

~3% whilst snowmelt decreased by ~5%. This occurred despite the model outputs indicating that these 2years have similar winter balances (Figure 7a,b), and occurs in other years following the most extreme negative balances (Figures S14–S16). In each of the subsequent years following the three most extreme negative mass balances, the relative contribution from glacier-ice melt is maximised (e.g., 66%–67% of annual discharge compared to 1980–2022 mean of 61%). Outside of the three most extreme years however, we find that the influence of a negative mass balance can be offset by variations in accumulation and ablation during the following year, resulting in no significant or consistent shift in the water budget.

Whilst we find evidence that the impact of a strongly negative mass balance can carry over into the following year in the most extreme cases, extreme positive mass-balance years in the 1980–2022 record (Figure 3) do not produce the same effect (Figures S17–S19). Following extreme positive years, the subsequent water budget still has a reduced fractional contribution from snowmelt and increased contribution from glacier-ice melt, despite having a larger than average accumulation area in the previous year. Relative contributions from glacier-ice melt are indeed minimised (e.g., 53%–54% of annual discharge compared to 1980–2022 mean of 61%) during the positive mass-balance years; however, the magnitude of the positive balances estimated for the period 1980–2022 is not high enough to exert an influence on the subsequent year.

4.4.2 | Quantifying Model Sensitivity to Climate

Acknowledging that the mass-balance model is structured to have a strong dependence on the temperature and accumulation inputs, we assess the sensitivity of modelled discharge to annual and seasonal air temperatures, accumulation, and mass balance to estimate how the runoff may change under future climate scenarios. By design in a temperature-index model, melt and thus discharge are both positively correlated with air temperature (Figure 8b,f). However, the enhanced temperature-index melt model is less sensitive to temperature than a classical degree-day model due to the inclusion of potential direct clear sky radiation in the degree-day factor (Hock 1999). Unsurprisingly, discharge is most strongly correlated with the mean summer (June–August) air temperature (Figure 8c,g). Modelled annual discharge averaged over the five warmest summers between 1980 and 2022 (87.2 $m^3\ s^{-1}$) was approximately double the average during the five coldest summers (43.8 $m^3\ s^{-1}$), with little change in the overall water budget (Figure 9a–c). During the warmest summer in the record (2004), modelled daily discharge reached a maximum of ~800 $m^3\ s^{-1}$, a significant increase compared to the average peak daily discharge over 1980–2022 (~530 $m^3\ s^{-1}$). The 2003–2004 hydrological year also saw the highest annual discharge during the study period: 100.5 $m^3\ s^{-1}$ compared to the 1980–2022 mean of 59.9 $m^3\ s^{-1}$, and the most negative mass balance (−1.41 m w.e. a^{-1}).

As summer air temperatures increase, the corresponding increase in annual discharge from glacier-ice melt is double that of snowmelt (8.38 $m^3\ s^{-1}°C^{-1}$ for glacier-ice melt vs. 4.18 $m^3\ s^{-1}°C^{-1}$ for snowmelt) (Figure 8c,g), due to the differences in the tuned radiation factors for snow and ice (Equation 1, Table S1). Annual discharge from glacier-ice melt and snowmelt are also both, unsurprisingly, inversely correlated with the annual mass balance (Figure 8a,e). In particular, glacier-ice melt shows a strong inverse correlation with the annual mass balance ($\rho = -0.98$), increasing by an estimated 23.1 $m^3\ s^{-1}$ for each 1 m w.e. decrease

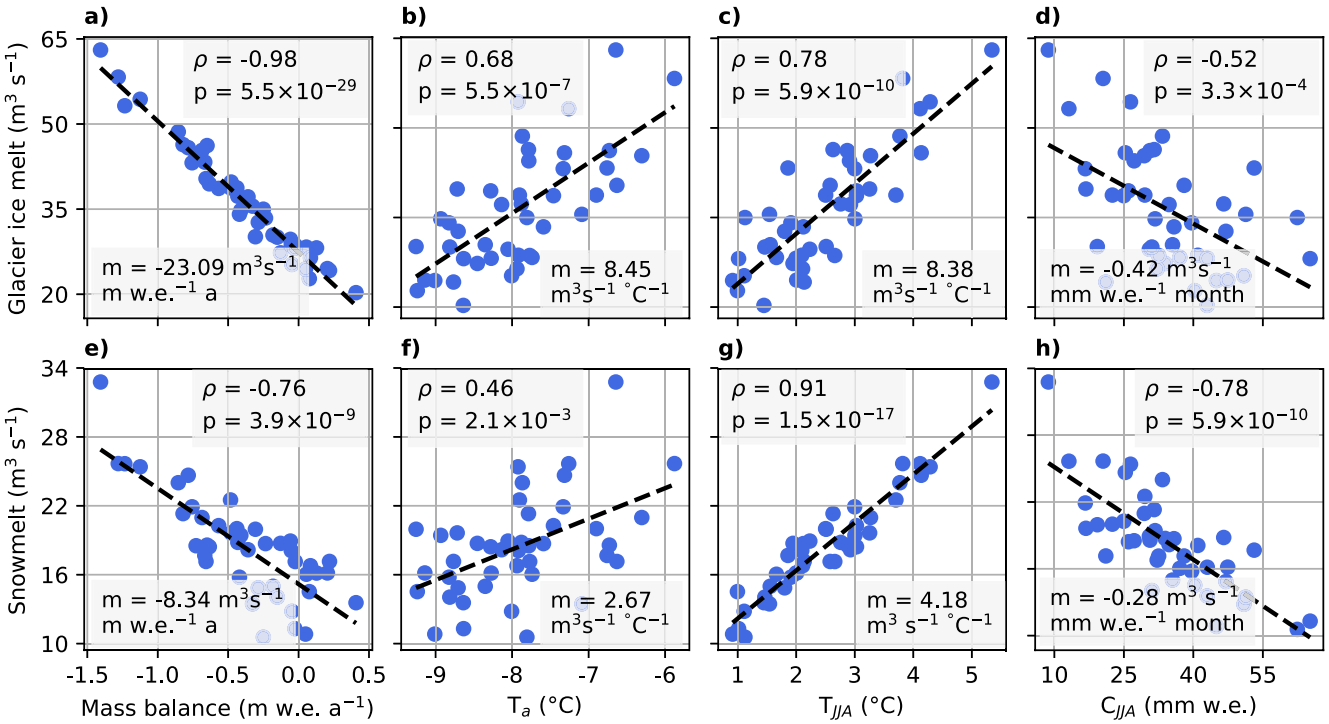

FIGURE 8 | Relationships between annual discharge from glacier-ice melt (a–d)/snowmelt (e–h) and: (a, e) mass balance, (b, f) mean annual air temperature (T_a), (c, g) mean summer air temperature (T_{JJA}), and (d, h) total summer accumulation (C_{JJA}), fitted with a linear regression. ρ is the Spearman's correlation coefficient, p is the p-value from Spearman's correlation test, and m is the slope of the regression line (dashed).

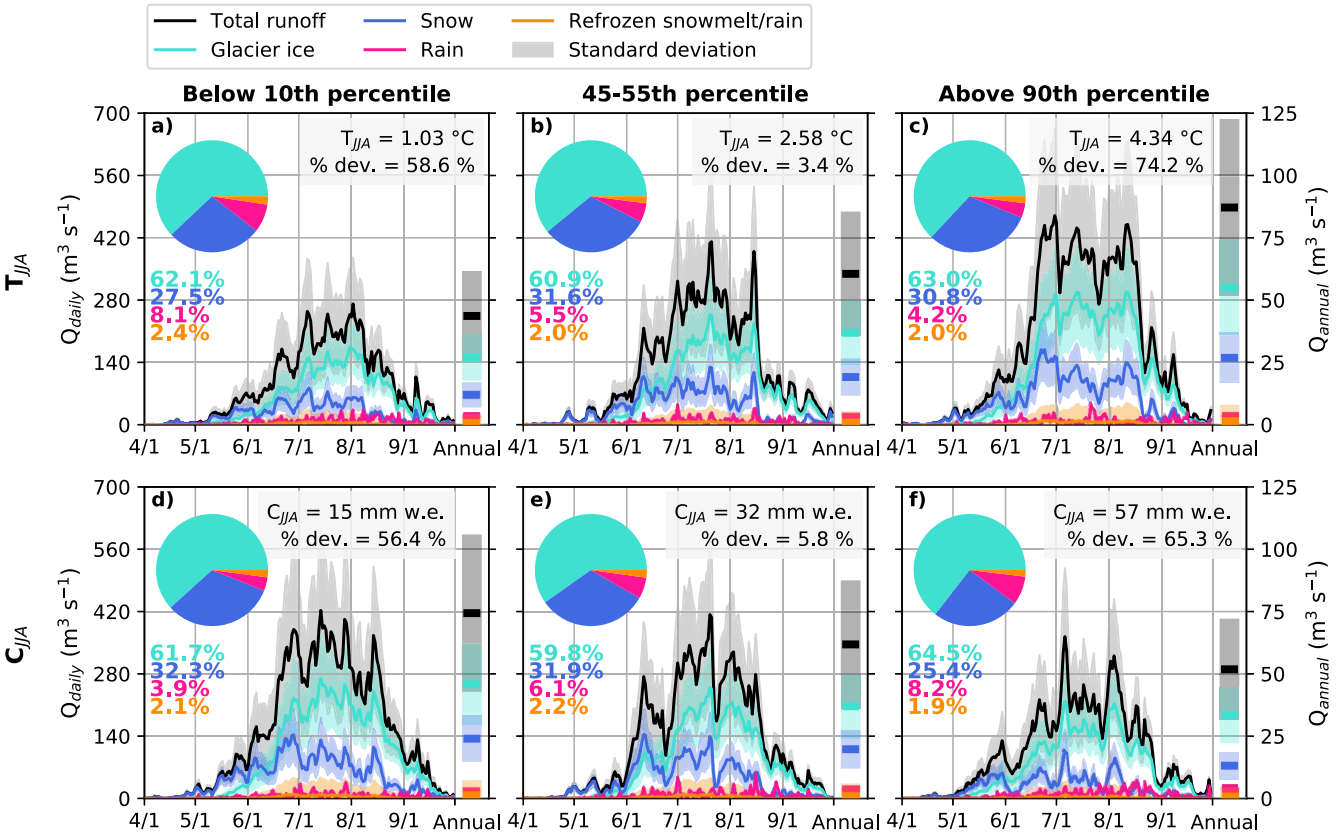

FIGURE 9 | Hydrographs corresponding to extremes in the summer temperature and accumulation record. Each hydrograph shown is the average of 5 years that fall (a, d) below the 10th percentile, (b, e) between the 45 and 55th percentile, and (c, f) above the 90th percentile of all years between 1980 and 2022. Percent deviation refers to deviation from the 1980 to 2022 mean summer temperature and accumulation.

in mass balance. This strong relationship is primarily due to the significant contribution of glacier-ice melt to net ablation (Figure 4b), whereas snowmelt contributes approximately half that of ice melt to net ablation.

Discharge from glacier-ice melt and snowmelt are inversely correlated with summer snowfall ($\rho = -0.52$ and $\rho = -0.78$, respectively; Figure 8d,h). Whilst high summer snowfall is associated with lower air temperatures, this relationship also captures the importance of summer snowfall on surface albedo (represented in the model by the constraint that the radiation factor for ice must be larger than that for snow). Summers with the least snowfall had, on average, higher annual discharge from glacier-ice melt by 12.7 m^3 s^{-1} compared to summers with the greatest snowfall (Figure 9d–f). In contrast, the mass balance over the winter season (i.e., the winter balance (Cogley et al. 2010)) is only weakly correlated with glacier-ice melt and has almost no correlation with snowmelt (Figure S20). This lack of correlation indicates that interannual variations in snowmelt contributions are more strongly influenced by the summer air temperatures than by winter precipitation.

To evaluate plausible changes to the melt sensitivities and their impact on future runoff, we estimate upper and lower bounds on the historical melt sensitivities from simulations that fall within 1–2 standard deviations above and below the geodetic balance target used in model tuning (see supplementary material). For glacier ice melt, we estimate a plausible range in the sensitivity to summer air temperatures of 6.46–10.37 m^3 $s^{-1}°C^{-1}$, and a range in the sensitivity to summer snowfall of −0.33 to −0.52 m^3 s^{-1} mm w.e.$^{-1}$ month. For snowmelt, we estimate a plausible range in the sensitivity to summer air temperature of 4.03–4.26 m^3 $s^{-1}°C^{-1}$, and a range in the sensitivity to summer snowfall of −0.27 to −0.29 m^3 s^{-1} mm w.e.$^{-1}$ month.

4.5 | Expected Changes to Runoff Based on Historical Sensitivities

Annual discharge from ice and snowmelt is most strongly correlated with summer air temperatures and inversely correlated with summer snowfall (Figure 8), compared to variations in spring, winter, and fall (Figure S20). As snowmelt and glacier-ice melt are historically the most important components of the water budget in the Kaskawulsh River headwaters (61% and 31% of annual catchment-wide discharge, Figure 4b), we expect that future changes in summer air temperature and summer snowfall will be important drivers of changes in discharge. Given the inherent uncertainties in future climate projections, our analysis is intended to generate hypotheses about future hydrological changes in the catchment based on the historical sensitivities to climate and the best available projections of future climate, rather than to provide precise predictions of runoff. Furthermore, the true sensitivity of runoff to the combined effects of temperature and snowfall is likely greater than its individually assessed sensitivity to temperature and snowfall, as presented here.

The CMIP6 projections for SSP5-8.5 indicate that summer air temperatures over the Kaskawulsh River headwaters are projected to increase by 1.42°C by 2021–2040, 2.55°C by 2041–2060, and 5.52°C by 2081–2100 relative to 1981–2010 (Figure 10). Assuming the sensitivity of annual glacier-ice melt to summer air temperature is stationary and equal to the historical (1980–2022) value (8.38 $m^3\ s^{-1}°C^{-1}$, Figure 8c), we estimate an increase in glacier-ice melt by a factor of 2.3 by 2081–2100 relative to the 1981–2010 modelled baseline.

By 2081–2100, summer snowfall in the catchment is projected to decrease by −25 mm w.e. $month^{-1}$ from June–August according to CMIP6 projections for SSP5-8.5. Again assuming the historical (1980–2022) sensitivity of annual glacier-ice melt to summer snowfall (−0.42 $m^3\ s^{-1}$ mm w.e.$^{-1}$ month, Figure 8d) is stationary, we estimate a minor increase in glacier-ice melt by a factor of 1.3 relative to the 1981–2010 modelled baseline (Figure 10) due to the decrease in summer snowfall. Variations in the snow and ice melt sensitivities (§4.4.2) lead to a range in our calculations of hypothetical future runoff of up to ±10.2 $m^3\ s^{-1}$ by 2081–2100 (Figure 10d).

Rainfall does not exhibit any statistically significant relationships with temperature over the historical period (Figure S21), so we assume no sensitivity for rainfall in our estimates of future discharge. However, CMIP6 projections indicate that total June–August precipitation is projected to increase by 19% by 2081–2100 compared to 1981–2010 under SSP5-8.5, and future temperature increases are expected to influence the partitioning precipitation into rain and snow (Gutiérrez et al. 2021). As rain accounts for just 2%–11% of the estimated annual water budget between 1980 and 2022 (Figure 4a), the impact of changes to rain/snow partitioning on the overall water budget are highly uncertain and will compete with increasing contributions from snow and ice melt. In addition to increased direct contributions to streamflow from rainfall, snowmelt also generally increases during rain-on-snow events (e.g., Marks et al. 2001; Kormos et al. 2014), which may become more common in the future as increasing air temperatures allow liquid precipitation to occur at higher elevations. There is also evidence that warming rates in this region are sensitive to elevation (Williamson et al. 2020), however our approach applies a uniform future change across the catchment which does not account for the potential variations in warming rates with elevation. In these estimates of future runoff we also assume no change in area of the Kaskawulsh Glacier, however future reductions in glacier area will inevitably influence runoff. Projections of the Kaskawulsh Glacier from a global glacier-modelling study (Rounce et al. 2023) suggest that this assumption should have minimal impact on our results

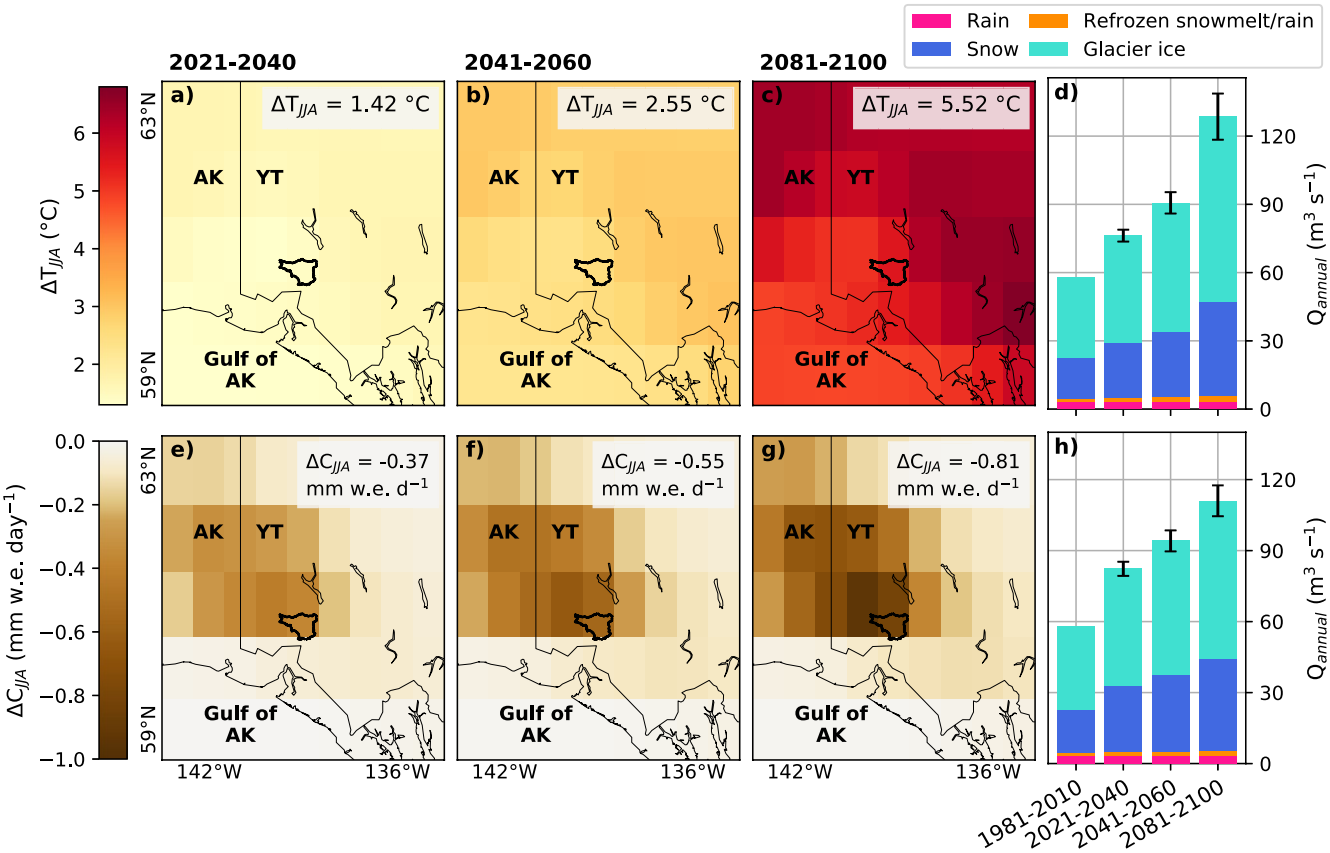

FIGURE 10 | Projections of future summer air-temperature change (ΔT_{JJA}) (a–c) and summer snowfall (ΔC_{JJA}) (e–g) from CMIP6 for SSP5-8.5 (Gutiérrez et al. 2021), with values from the gridcell with the greatest overlap with the Kaskawulsh River headwaters (thick black outline) printed in the top right corner of each panel. (d, h): Historical discharge (1981–2010) estimated in this study, and hypothetical future discharge estimated individually for changes in summer air temperature (d) and summer snowfall (h). Future estimates are computed by multiplying the historical sensitivities (Figure 8) by the projected changes for the three future time periods and adding the result to modelled 1981–2010 discharge (Figure 4a). Vertical bars represent results from a range of melt sensitivities estimated from a subset of simulations in the model ensemble that fall within 1–2 standard deviations above and below the geodetic balance target used in model tuning.

within the remainder of the century: whilst a ~46% reduction in glacier mass is projected by 2100 relative to 2001–2020 under SSP5-8.5, this is accompanied by only a 7.5% reduction in glacier area, equivalent to ~79 km^2. The same projections indicate that runoff from the Kaskawulsh Glacier will likely continue to increase through the remainder of the century, with peak water not expected to occur until after 2100.

5 | Discussion

5.1 | Regional Glacier Mass Loss

Several other studies have estimated mass loss in the region through a variety of methods, both individually for the Kaskawulsh Glacier (e.g., Larsen et al. 2015; Berthier et al. 2010; Foy et al. 2011) and at the regional scale (e.g., Hugonnet et al. 2021) for periods bracketed by our study period. The mass loss of Kaskawulsh Glacier that we estimate from 1995 to 2013 (-0.38 ± 0.16 m w.e. a^{-1}) agrees within uncertainty with that estimated by Larsen et al. (2015) for the same period using repeat laser altimetry (-0.35 m w.e. a^{-1}). Our 1979–2007 estimate (-0.33 ± 0.15 m w.e. a^{-1}) is also in agreement within uncertainty with the 1977–2007 geodetic estimate from Berthier et al. (2010) (-0.46 ± 0.20 m w.e. a^{-1}).

The St. Elias Mountains alone represent about 38% of the total glacierized area of 33 174 km^2 in the Yukon–Alaska region (Randolph Glacier Inventory, version 6.0) (Arendt et al. 2017) and have experienced an estimated mass change rate of −23.3 Gt a^{-1} from 2000 to 2019 (Hugonnet et al. 2021) (35% of the Yukon–Alaska regional mass loss). The Kaskawulsh River Headwaters represent 3.5% of the glacier area in the St. Elias Mountains, but just 2.2% of the estimated 2000–2019 mass loss, based on our model results (-0.52 ± 0.17 Gt a^{-1}). This finding is not unexpected, given the geographic location of the catchment on the continental side of the range, where glaciers are under-contributing to regional mass loss relative to their maritime counterparts (e.g., Jakob et al. 2020; Jin et al. 2017). Mass loss from coastal glaciers and icefields may also be accelerating faster than continental glaciers like those in the Kaskawulsh River headwaters. The western (coastal) watershed of the Juneau Icefield, for example, had an estimated mass balance of -0.81 ± 0.11 m w.e. a^{-1} from 1980 to 2016 (Young et al. 2021b). Icefield-wide mass-balance decreased from -0.21 m a^{-1} in the 2000s to -0.74 m a^{-1} in the 2010s (Davies et al. 2024), a greater rate of change compared to the decrease from -0.45 m w.e. a^{-1} to -0.49 m w.e. a^{-1} in the Kaskawulsh River headwaters over the same period (Table 2).

5.2 | Hydrological Changes Across the Yukon and Alaska

The hydrological regime of the Kaskawulsh River headwaters is strongly influenced by glacier ice melt, which accounts for an average of 61% of the annual catchment-wide discharge from 1980 to 2022 (Figure 4b). Interannual discharge variability decreased over 1980–2022, a natural consequence of the progression towards peak water and a trend that, along with the increase in discharge from ice melt (Figure 5), signifies the increasing influence of ice melt on the water budget. The nearby White River watershed in southwest Yukon (30% glacierized) exhibits a similar trend, where increasing ablation-season discharge and decreasing discharge variability over 1974–2008 indicate the watershed has not yet passed peak water (Chesnokova et al. 2020). As the Kaskawulsh Glacier retreats and ultimately passes peak water in the future, we can expect interannual discharge variability to increase as the glacier exerts a progressively weaker influence on catchment-wide discharge (e.g., Baraër et al. 2012), making the discharge from the catchment more sensitive to interannual climate variability.

Future changes in glacier extent and mass balance may also produce shifts in the timing of runoff in this region (e.g., Huss and Hock 2018). We estimate that the onset of glacier ice melt occurred earlier in the melt season by 3.5 days per decade from 1980–2022, producing an increase in spring runoff that has been reported in other glacierized watersheds yet to pass peak water, such as the western Juneau Icefield (Young et al. 2021b). Discharge from glacier ice melt in the Kaskawulsh River headwaters also increased during July and August (Figure 5), although future glacier mass loss could eventually lead to decreased runoff contributions in late summer. Relative to the period 1990–2010, monthly glacier runoff in the Alsek River basin is projected to increase by 28% in June and decrease by 7% in August by the end of the century (2080–2100) under RCP4.5 (Huss and Hock 2018). In the Copper River basin in south-central Alaska, Mizukami et al. (2022) predict that spring runoff will increase by the end of the century due to increased snowmelt, whilst summer runoff will be significantly reduced due to glacier loss. The Gulf of Alaska watershed, to which the Alsek River basin and Copper River basin are both major contributors (Neal et al. 2010), is strongly influenced by glacier ice melt, which accounted for 17% of the mean annual discharge between 1980 and 2014 (Beamer et al. 2016). Nearly half of all freshwater discharge to the Gulf of Alaska originates from glacierized areas (Neal et al. 2010), highlighting the potential impact of shifts in the timing and volume of runoff from highly glacierized catchments such as the Kaskawulsh River headwaters.

5.3 | Future Outlook and Downstream Impacts

In the short term, increasing discharge in the Kaskawulsh River headwaters may increase downstream sediment transport and erosion (Milner et al. 2017), and elevate the potential for geohazards such as high peak annual discharge and floods (e.g., Ragettli et al. 2016). Based on the strong historical correlation between summer air temperature and ice and snowmelt (Figure 8c,g), we also anticipate that changes in summer air temperature will likely have a large impact on future discharge in this region (Figure 10). High correlations between summer air temperatures and ice melt have been reported for other continental glaciers in western North America (e.g., O'Neel et al. 2014; Fleming and Clarke 2003; Moore and Demuth 2001), in contrast to coastal glaciers, which are typically influenced by large seasonal snowpacks and significant summer rainfall which contribute more consistently to discharge (e.g., O'Neel et al. 2014).

Discharge from the Kaskawulsh River headwaters is also strongly inversely correlated with the annual glacier mass

balance (Figure 8a,e); however, this correlation is predominantly related to the correlation between discharge and ablation. In some cases, an extremely negative balance can result in excess ice melt in the following year due to a depletion of the multi-year snowpack above the equilibrium line (Figure 7). On the Columbia Glacier in Washington, USA, three consecutive years of significant negative annual balances from 2003 to 2005 led to a similar mode of mass loss with a more extreme outcome: the complete loss of the accumulation zone and significant thinning at high elevations following the period of strong negative balances (Pelto 2011). In contrast with the effect of extreme negative balance years, we find no examples of positive mass balances in our modelled record high enough to inhibit ice melt during the following ablation season, unlike for the maritime Wolverine Glacier in Alaska where winter accumulation has been known to reduce mass loss during the following ablation season (O'Neel et al. 2014). We therefore expect that future mass changes of the Kaskawulsh Glacier will be primarily driven by temperature rather than precipitation.

Although changes in glacier area are not incorporated in the mass-balance model, projections suggest that the Kaskawulsh Glacier will experience limited retreat relative to its current size during the remainder of the century, with an estimated area loss of 7.5% by 2100 relative to 2001–2020 under SSP5-8.5 (Rounce et al. 2023). This is consistent with the glacier's substantial ice thickness in the terminus region (~400–600 m) (Main et al. 2023), the presence of widespread insulating debris cover (Robinson et al. 2025), and the glacier's historically slow response to mass imbalance (e.g., Young et al. 2021a; Foy et al. 2011). In northwest British Columbia and southwest Yukon, the dominant mode of glacier mass loss in response to an increase in temperature thus far has been thinning without significant terminus retreat (e.g., Moore et al. 2009). As the Kaskawulsh Glacier continues to thin, the surface-elevation lowering can expose the glacier to warmer temperatures at lower elevations and enhance surface melt. Until sustained thinning of the terminus region of the Kaskawulsh Glacier (e.g., Main et al. 2023) leads to significant retreat, this surface-elevation feedback may amplify meltwater production, further influencing the water budget.

6 | Conclusions

This study employs a mass-balance model driven by downscaled and bias-corrected climate reanalysis data to estimate the glacier mass loss, discharge, and water budget of the Kaskawulsh River headwaters over four decades from 1980 to 2022. We conduct statistical analyses on timeseries of modelled temperature, precipitation, and discharge to quantify temporal trends and identify correlations between climatic and discharge variables with which we estimate the sensitivity of modelled runoff to climate change.

Glaciers in the Kaskawulsh River headwaters are estimated to have lost 18.02 Gt of mass between 1980 and 2022 (−0.38 m w.e. a^{-1}), accounting for 2.2% of the estimated mass loss in the St. Elias Mountains as a whole between 2000 and 2019, an under-contribution given that these glaciers represent 3.5% of the total glacierized area in the St. Elias Mountains. Since the 1980s the average annual mass-loss rate has increased with each subsequent decade, more than doubling from −0.22 ±0.13 m w.e. a^{-1} from 1980 to 1989 to −0.49 ±0.17 m w.e. a^{-1} from 2010 to 2019. The rerouting of meltwater from the Ä'äy Chù to the Kaskawulsh River in 2016 produced a substantial increase in discharge in the Alsek River, with discharge from the Kaskawulsh River Headwaters accounting for an estimated 22%–29% of the annual discharge measured at the downstream hydrometric station on the Alsek River above Bates River after 2016 and 3%-7% of the annual discharge from the Alsek River to the Gulf of Alaska.

Mean ablation season (May–August) discharge from glacier-ice melt increased at a statistically-significant rate of 7.7 $m^3\ s^{-1}$ per decade, accompanied by shifts in the timing of discharge. The onset of discharge from glacier-ice melt occurred an estimated 3.5 days earlier per decade and the onset of net ablation in the catchment (the date when the annual cumulative balance becomes negative) occurred approximately 5 days earlier per decade over 1980–2022. Meanwhile, the annual variability of glacier-ice melt discharge (and total discharge) decreased. These trends are evidence that the Kaskawulsh River headwaters is in the early stages of progressing towards "peak water" (Baraër et al. 2012). Mean ablation-season discharge from rain also increased at a statistically significant rate of 1.0 $m^3\ s^{-1}$ per decade ($p = 0.002$), an indication that rainfall may become an increasingly important component of the water budget in the future, especially in August and September.

The annual water budget varies depending on temperature and precipitation, with glacier-ice melt accounting for 53%–67% (mean of 61%) of annual catchment-wide discharge, snowmelt accounting for 20%–38% (mean of 31%), rain accounting for 2%–11% (mean of 6%), and melt from refrozen snowmelt/rain accounting for 1%–3% (mean of 2%). We find that maximum contributions from glacier-ice melt (66%–67%) to annual discharge typically occur in the year following an extreme negative mass-balance year. This result suggests that a significant increase in the equilibrium line altitude can precondition the glacier surface for enhanced ice melt the following summer. High rates of summer snowfall may serve to dampen ice melt by temporarily increasing the surface albedo, however, summer snowfall rates are projected to decrease in the future along with a concurrent increase in summer temperatures. We hypothesise a more than doubling (2.3×) of annual runoff by 2080–2100 based summer air-temperature increases projected by CMIP6 (SSP5-8.5) and the sensitivity of modelled runoff to summer air temperature calculated over the historical period of 1980–2022.

Other large glaciers in the region will likely undergo comparable hydrological changes driven by ongoing climate change, whilst smaller glaciers may already be experiencing a post-peak-water decline in runoff. The resulting shifts in the hydrological system are expected to affect streamflow and temperature, alter sediment and nutrient delivery to aquatic ecosystems (e.g., Hood and Berner 2009), and impact habitat conditions for key species such as salmon (e.g., Moore et al. 2023; Pitman et al. 2021). Coupled mass-balance and ice-dynamics model projections are needed to simulate the competing effects of glacier area loss and enhanced melt under future warming scenarios. A broader investigation of this nature will help provide a more comprehensive picture of the regional hydrological response to climate change, from

which we can begin to anticipate the downstream ecological, environmental, and socioeconomic impacts.

Acknowledgements

The Kaskawulsh River headwaters study site is located within the Traditional Territories of the Kluane, Champagne & Aishihik, and White River First Nations. We thank E. Berthier for providing the DEMs used in downscaling and helping with the interpretation, E. Young for providing the original downscaling and melt-model code and for helping with many aspects of using the model, and B. Tober for providing the future projections of glacier area change for the Kaskawulsh Glacier. Katherine M. Robinson and Gwenn E. Flowers are grateful for financial support provided by the Natural Sciences and Engineering Research Council of Canada, Simon Fraser University, and Environment and Climate Change Canada. Michel Baraër was supported by the Natural Sciences and Engineering Research Council of Canada under grant Nos. RGPIN-2020-05612 and RGPNS-2020-05612. David R. Rounce was supported by NASA under grant Nos. 80NSSC20K1296 and 80NSSC20K1595.

Data Availability Statement

The Hock (1999) Distributed Enhanced Temperature Index Model (DETIM) shading module code used to calculate the potential direct clear-sky solar radiation was downloaded from http://regine.github.io/meltmodel/. Daily and annual discharge data from the Dezadeash River and Alsek River above Bates River hydrometric stations were downloaded from the Environment and Climate Change Canada Historical Hydrometric Data web site: https://wateroffice.ec.gc.ca/mainmenu/historical_data_index_e.html. Daily discharge data from the Alsek River at Dry Bay near Yakutat station were obtained from the United States Geological Survey: https://waterdata.usgs.gov/monitoring-location/15129120. The Kaskawulsh Glacier outline was obtained from https://www.glims.org/maps/glims. The raw NARR data downscaled for this study were obtained from https://downloads.psl.noaa.gov/Datasets/NARR. Downscaled and bias-corrected temperature data for the Kaskawulsh River Headwaters can be found at: https://doi.org/10.5281/zenodo.14010407, and downscaled and bias-corrected precipitation data can be found at: https://doi.org/10.5281/zenodo.14014495. Other inputs used to run the mass-balance model can be downloaded at: https://doi.org/10.5281/zenodo.14010158. The model outputs (spanning 1980–2022) used to conduct the analyses presented in this paper can be downloaded at: https://doi.org/10.5281/zenodo.14010257. Downscaling, bias correction, model tuning, and melt-model scripts are available at https://doi.org/10.5281/zenodo.14635182.

References

Arendt, A., A. Bliss, T. Bolch, et al. 2017. Randolph Glacier Inventory–A Dataset of Global Glacier Outlines: Version 6.0: Technical Report, Global Land Ice Measurements from Space.

Azam, M. F., and S. Srivastava. 2020. "Mass Balance and Runoff Modelling of Partially Debris-Covered Dokriani Glacier in Monsoon-Dominated Himalaya Using ERA5 Data Since 1979." *Journal of Hydrology* 590: 125432. https://doi.org/10.1016/j.jhydrol.2020.125432.

Bachelder, J., M. Cadieux, C. Liu-Kang, et al. 2020. "Chemical and Microphysical Properties of Wind-Blown Dust Near an Actively Retreating Glacier in Yukon, Canada." *Aerosol Science and Technology* 54, no. 1: 2–20.

Baraër, M., B. G. Mark, J. M. McKenzie, et al. 2012. "Glacier Recession and Water Resources in Peru's Cordillera Blanca." *Journal of Glaciology* 58, no. 207: 134–150.

Beamer, J., D. Hill, A. Arendt, and G. Liston. 2016. "High-Resolution Modeling of Coastal Freshwater Discharge and Glacier Mass Balance in the Gulf of Alaska Watershed." *Water Resources Research* 52, no. 5: 3888–3909.

Berthier, E., E. Schiefer, G. K. C. Clarke, B. Menounos, and F. Rémy. 2010. "Contribution of Alaskan Glaciers to Sea-Level Rise Derived From Satellite Imagery." *Nature Geoscience* 3, no. 2: 92–95. https://doi.org/10.1038/ngeo737.

Bliss, A., R. Hock, and V. Radić. 2014. "Global Response of Glacier Runoff to Twenty-First Century Climate Change." *Journal of Geophysical Research: Earth Surface* 119, no. 4: 717–730. https://doi.org/10.1002/2013JF002931.

Brabets, T. P., and M. A. Walvoord. 2009. "Trends in Streamflow in the Yukon River Basin From 1944 to 2005 and the Influence of the Pacific Decadal Oscillation." *Journal of Hydrology* 371, no. 1–4: 108–119.

Chesnokova, A., M. Baraër, T. Laperrière-Robillard, and K. Huh. 2020. "Linking Mountain Glacier Retreat and Hydrological Changes in Southwestern Yukon." *Water Resources Research* 56, no. 1: e2019WR025706. https://doi.org/10.1029/2019WR025706.

Clarke, G. K. C., and G. Holdsworth. 2002. *Glaciers of the St. Elias Mountains*. US Geological Survey Professional Paper.

Cogley, J. G., A. Arendt, A. Bauder, et al. 2010. "Glossary of Glacier Mass Balance and Related Terms." IHP-VII Technical Documents in Hydrology No. 86, IACS Contribution No. 2, UNESCO-IHP, Paris.

Criscitiello, A. S., M. A. Kelly, and B. Tremblay. 2010. "The Response of Taku and Lemon Creek Glaciers to Climate." *Arctic, Antarctic, and Alpine Research* 42, no. 1: 34–44.

Davies, B., R. McNabb, J. Bendle, et al. 2024. "Accelerating Glacier Volume Loss on Juneau Icefield Driven by Hypsometry and Melt-Accelerating Feedbacks." *Nature Communications* 15, no. 1: 5099.

Farinotti, D., M. Huss, J. J. Fürst, et al. 2019. "A Consensus Estimate for the Ice Thickness Distribution of all Glaciers on Earth." *Nature Geoscience* 12, no. 3: 168–173. https://doi.org/10.1038/s41561-019-0300-3.

Fleming, S. W., and G. K. C. Clarke. 2003. "Glacial Control of Water Resource and Related Environmental Responses to Climatic Warming: Empirical Analysis Using Historical Streamflow Data From Northwestern Canada." *Canadian Water Resources Journal* 28, no. 1: 69–86.

Foy, N., L. Copland, C. Zdanowicz, M. Demuth, and C. Hopkinson. 2011. "Recent Volume and Area Changes of Kaskawulsh Glacier, Yukon, Canada." *Journal of Glaciology* 57, no. 203: 515–525. https://doi.org/10.3189/002214311796905596.

Gidden, M. J., K. Riahi, S. J. Smith, et al. 2019. "Global Emissions Pathways Under Different Socioeconomic Scenarios for Use in CMIP6: A Dataset of Harmonized Emissions Trajectories Through the End of the Century." *Geoscientific Model Development* 12, no. 4: 1443–1475.

Goss, G. A. 2021. "Glacier Retreat and Fluvial Landscape Response." PhD thesis, University of Calgary.

Guan, H., J. L. Wilson, and H. Xie. 2009. "A Cluster-Optimizing Regression-Based Approach for Precipitation Spatial Downscaling in Mountainous Terrain." *Journal of Hydrology* 375, no. 3–4: 578–588. https://doi.org/10.1016/j.jhydrol.2009.07.007.

Gutiérrez, J., R. Jones, G. Narisma, et al. 2021. "Atlas." In *Climate Change 2021: The Physical Science Basis. Contribution of Working Group I to the Sixth Assessment Report of the Intergovernmental Panel on Climate Change*. Cambridge University Press.

Hamed, K. H., and A. R. Rao. 1998. "A Modified Mann-Kendall Trend Test for Autocorrelated Data." *Journal of Hydrology* 204, no. 1–4: 182–196. https://doi.org/10.1016/s0022-1694(97)00125-x.

Hock, R. 1999. "A Distributed Temperature-Index Ice-and Snowmelt Model Including Potential Direct Solar Radiation." *Journal of Glaciology* 45, no. 149: 101–111. https://doi.org/10.3189/S0022143000003087.

Hood, E., and L. Berner. 2009. "Effects of Changing Glacial Coverage on the Physical and Biogeochemical Properties of Coastal Streams in Southeastern Alaska." *Journal of Geophysical Research: Biogeosciences* 114, no. G3: G03001.

Huck, R., R. G. Bryant, and J. King. 2023. "The (Mis)identification of High-Latitude Dust Events Using Remote Sensing Methods in the Yukon, Canada: A Sub-Daily Variability Analysis." *Atmospheric Chemistry and Physics* 23, no. 11: 6299–6318.

Hugonnet, R., R. McNabb, E. Berthier, et al. 2021. "Accelerated Global Glacier Mass Loss in the Early Twenty-First Century." *Nature* 592, no. 7856: 726–731. https://doi.org/10.1038/s41586-021-03436-z.

Hunter, C., R. Moore, and I. McKendry. 2020. "Evaluation of the North American Regional Reanalysis (NARR) Precipitation Fields in a Topographically Complex Domain." *Hydrological Sciences Journal* 65, no. 5: 786–799. https://doi.org/10.1080/02626667.2019.1591624.

Huss, M., and R. Hock. 2018. "Global-Scale Hydrological Response to Future Glacier Mass Loss." *Nature Climate Change* 8, no. 2: 135–140. https://doi.org/10.1038/s41558-017-0049-x.

IPCC. 2021. "Climate Change 2021: The Physical Science Basis." In *Contribution of Working Group I to the Sixth Assessment Report of the Intergovernmental Panel on Climate Change*. Cambridge University Press.

Jakob, L., N. Gourmelen, M. Ewart, and S. Plummer. 2020. Ice Loss in High Mountain Asia and the Gulf of Alaska Observed by CryoSat-2 Swath Altimetry Between 2010 and 2019.

Janssens, I., and P. Huybrechts. 2000. "The Treatment of Meltwater Retention in Mass-Balance Parameterizations of the Greenland Ice Sheet." *Annals of Glaciology* 31: 133–140. https://doi.org/10.3189/172756400781819941.

Jarosch, A. H., F. S. Anslow, and G. K. C. Clarke. 2012. "High-Resolution Precipitation and Temperature Downscaling for Glacier Models." *Climate Dynamics* 38: 391–409. https://doi.org/10.1007/s00382-010-0949-1.

Jin, S., T. Zhang, and F. Zou. 2017. "Glacial Density and GIA in Alaska Estimated From ICESat, GPS and GRACE Measurements." *Journal of Geophysical Research: Earth Surface* 122, no. 1: 76–90.

Josberger, E. G., W. R. Bidlake, R. S. March, and B. W. Kennedy. 2007. "Glacier Mass-Balance Fluctuations in the Pacific Northwest and Alaska, USA." *Annals of Glaciology* 46: 291–296.

Kendall, M. G. 1948. *Rank Correlation Methods*. Griffin.

Kormos, P. R., D. Marks, J. P. McNamara, H. Marshall, A. Winstral, and A. N. Flores. 2014. "Snow Distribution, Melt and Surface Water Inputs to the Soil in the Mountain Rain–Snow Transition Zone." *Journal of Hydrology* 519: 190–204.

La Frenierre, J., and B. G. Mark. 2014. "A Review of Methods for Estimating the Contribution of Glacial Meltwater to Total Watershed Discharge." *Progress in Physical Geography* 38, no. 2: 173–200. https://doi.org/10.1177/0309133313516161.

Larsen, C., E. Burgess, A. Arendt, S. O'neel, A. Johnson, and C. Kienholz. 2015. "Surface Melt Dominates Alaska Glacier Mass Balance." *Geophysical Research Letters* 42, no. 14: 5902–5908.

Li, J., F. Rodriguez-Morales, X. Fettweis, et al. 2023. "Snow Stratigraphy Observations From Operation IceBridge Surveys in Alaska Using S and C Band Airborne Ultra-Wideband FMCW (Frequency-Modulated Continuous Wave) Radar." *Cryosphere* 17, no. 1: 175–193. https://doi.org/10.5194/tc-17-175-2023.

Li, Z., X. Shi, Q. Tang, et al. 2020. "Partitioning the Contributions of Glacier Melt and Precipitation to the 1971–2010 Runoff Increases in a Headwater Basin of the Tarim River." *Journal of Hydrology* 583: 124579. https://doi.org/10.1016/j.jhydrol.2020.124579.

Main, B., L. Copland, B. Smeda, et al. 2023. "Terminus Change of Kaskawulsh Glacier, Yukon, Under a Warming Climate: Retreat, Thinning, Slowdown and Modified Proglacial Lake Geometry." *Journal of Glaciology* 69, no. 276: 936–952. https://doi.org/10.1017/jog.2022.114.

Mann, H. B. 1945. "Nonparametric Tests Against Trend." *Econometrica: Journal of the Econometric Society* 13, no. 3: 245–259.

Mantua, N. J., and S. R. Hare. 2002. "The Pacific Decadal Oscillation." *Journal of Oceanography* 58: 35–44.

Marks, D., T. Link, A. Winstral, and D. Garen. 2001. "Simulating Snowmelt Processes During Rain-On-Snow Over a Semi-Arid Mountain Basin." *Annals of Glaciology* 32: 195–202.

Mesinger, F., G. DiMego, E. Kalnay, et al. 2006. "North American Regional Reanalysis." *Bulletin of the American Meteorological Society* 87, no. 3: 343–360. https://doi.org/10.1175/BAMS-87-3-343.

Milner, A. M., K. Khamis, T. J. Battin, et al. 2017. "Glacier Shrinkage Driving Global Changes in Downstream Systems." *Proceedings of the National Academy of Sciences* 114, no. 37: 9770–9778.

Mizukami, N., A. J. Newman, J. S. Littell, et al. 2022. "New Projections of 21st Century Climate and Hydrology for Alaska and Hawai'i." *Climate Services* 27: 100312.

Moore, J. W., K. J. Pitman, D. Whited, et al. 2023. "Mining Stakes Claim on Salmon Futures as Glaciers Retreat." *Science* 382, no. 6673: 887–889.

Moore, R., and M. Demuth. 2001. "Mass Balance and Streamflow Variability at Place Glacier, Canada, in Relation to Recent Climate Fluctuations." *Hydrological Processes* 15, no. 18: 3473–3486.

Moore, R., S. Fleming, B. Menounos, et al. 2009. "Glacier Change in Western North America: Influences on Hydrology, Geomorphic Hazards and Water Quality." *Hydrological Processes: An International Journal* 23, no. 1: 42–61.

Neal, E. G., E. Hood, and K. Smikrud. 2010. "Contribution of Glacier Runoff to Freshwater Discharge Into the Gulf of Alaska." *Geophysical Research Letters* 37, no. 6: L06404. https://doi.org/10.1029/2010GL042385.

O'Neel, S., E. Hood, A. Arendt, and L. Sass. 2014. "Assessing Streamflow Sensitivity to Variations in Glacier Mass Balance." *Climatic Change* 123: 329–341.

Pelto, M. 2011. "Skykomish River, Washington: Impact of Ongoing Glacier Retreat on Streamflow." *Hydrological Processes* 25, no. 21: 3356–3363.

Pitman, K. J., J. W. Moore, M. Huss, et al. 2021. "Glacier Retreat Creating New Pacific Salmon Habitat in Western North America." *Nature Communications* 12, no. 1: 6816. https://doi.org/10.1038/s41467-021-26897-2.

Ragettli, S., W. W. Immerzeel, and F. Pellicciotti. 2016. "Contrasting Climate Change Impact on River Flows From High-Altitude Catchments in the Himalayan and Andes Mountains." *Proceedings of the National Academy of Sciences* 113, no. 33: 9222–9227.

RGI Consortium. 2017. Randolph Glacier Inventory–A Dataset of Global Glacier Outlines: Version 6.0: Technical Report, Global Land Ice Measurements from Space.

Robinson, K. 2024. "Reconstructing a Multi-Decadal Runoff Record for a Highly-Glacierized Catchment in Yukon, Canada." Master's thesis, Simon Fraser University.

Robinson, K. M., G. E. Flowers, and D. R. Rounce. 2025. "Sensitivity of Modelled Mass Balance and Runoff to Representations of Debris and Accumulation on the Kaskawulsh Glacier, Yukon, Canada." *Journal of Glaciology* 71: e42. https://doi.org/10.1017/jog.2025.8.

Rounce, D. R., R. Hock, F. Maussion, et al. 2023. "Global Glacier Change in the 21st Century: Every Increase in Temperature Matters." *Science* 379, no. 6627: 78–83. https://doi.org/10.1126/science.abo1324.

Sen, P. K. 1968. "Estimates of the Regression Coefficient Based on Kendall's Tau." *Journal of the American Statistical Association* 63, no. 324: 1379–1389.

Shugar, D. H., J. J. Clague, J. L. Best, et al. 2017. "River Piracy and Drainage Basin Reorganization Led by Climate-Driven Glacier Retreat." *Nature Geoscience* 10, no. 5: 370–375. https://doi.org/10.1038/ngeo2932.

Spearman, C. 1904. "The Proof and Measurement of Association Between Two Things." *American Journal of Psychology* 15: 88.

Wheler, B. A., and G. E. Flowers. 2011. "Glacier Subsurface Heat-Flux Characterizations for Energy-Balance Modelling in the Donjek Range, Southwest Yukon, Canada." *Journal of Glaciology* 57, no. 201: 121–133. https://doi.org/10.3189/002214311795306709.

Williamson, S. N., C. Zdanowicz, F. S. Anslow, et al. 2020. "Evidence for Elevation-Dependent Warming in the st. Elias Mountains, Yukon, Canada." *Journal of Climate* 33, no. 8: 3253–3269.

Young, E. M., G. E. Flowers, E. Berthier, and R. Latto. 2021a. "An Imbalancing Act: The Delayed Dynamic Response of the Kaskawulsh Glacier to Sustained Mass Loss." *Journal of Glaciology* 67, no. 262: 313–330. https://doi.org/10.1017/jog.2020.107.

Young, J. C., E. Pettit, A. Arendt, E. Hood, G. E. Liston, and J. Beamer. 2021b. "A Changing Hydrological Regime: Trends in Magnitude and Timing of Glacier Ice Melt and Glacier Runoff in a High Latitude Coastal Watershed." *Water Resources Research* 57, no. 7: e2020WR027404. https://doi.org/10.1029/2020WR027404.

Zemp, M., M. Huss, E. Thibert, et al. 2019. "Global Glacier Mass Changes and Their Contributions to Sea-Level Rise From 1961 to 2016." *Nature* 568, no. 7752: 382–386. https://doi.org/10.1038/s41586-019-1071-0.

Supporting Information

Additional supporting information can be found online in the Supporting Information section.